# PICKING UP STEAM: A YEAR LONG INFRASONIC RECORD OF STEAMBOAT GEYSER. MINOR AND MAJOR PAROXYSMS OF MULTI-PHASE ERUPTIONS AT STEAMBOAT GEYSER, YELLOWSTONE NATIONAL PARK

by

Margaret Holahan

A thesis

submitted in partial fulfillment

of the requirements for the degree of

Master of Science in Geoscience

Boise State University

August 2023

BOISE STATE UNIVERSITY GRADUATE COLLEGE

# DEFENSE COMMITTEE AND FINAL READING APPROVALS

of the thesis submitted by

Margaret Holahan

Thesis Title: Picking Up Steam: A Year Long Infrasonic Record of Steamboat Geyser. Minor and Major Paroxysms of the Multi-Phase Eruptions at Steamboat Geyser, Yellowstone National Park

Date of Final Oral Examination: 24 February 2023

The following individuals read and discussed the thesis submitted by student Margaret Holahan, and they evaluated her presentation and response to questions during the final oral examination. They found that the student passed the final oral examination.

| | |
|---|---|
| Jeffrey B. Johnson, Ph.D. | Chair, Supervisory Committee |
| Lee Liberty, M.S. | Member, Supervisory Committee |
| Michael Poland, Ph.D. | Member, Supervisory Committee |

The final reading approval of the thesis was granted by Jeffrey B. Johnson, Ph.D., Chair of the Supervisory Committee. The thesis was approved by the Graduate College.

ACKNOWLEDGMENTS

Committee members: Jeff Johnson, Lee Liberty and Mike Poland. External University collaborators: Dr. Jamie Farrell and Mara Reed. Field assistants: Tamara Satterwhite, Ashley Bosa, Armando Pindea, Ella Johnson, and Christine Sandbach. Yellowstone National Park Research Staff: Annie Carlson, Jeff Hungerford, Morgan Nasholds, and Megan Norr. BSU Infrasound Lab. Geyser Times

ABSTRACT

The renewed activity of the world's tallest geyser, Steamboat Geyser (Yellowstone National Park) in 2018, offers the opportunity to utilize long-term continuous infrasound and low-frequency acoustic monitoring to quantify eruptive behaviors. Eruption parameters including onset timing, duration, phase transitions between steam and water, instantaneous sound intensity, eruptive power, energy content, and spectral character, may be used to characterize individual eruption styles and reveal eruption trends. I interpret the character of the acoustic radiation through corroboration of first-hand observations and time-lapse video. I find that infrasound (acoustic energy below 20 Hz) is a particularly effective tool for tracking the evolving eruption style of Steamboat and complements other monitoring techniques data streams including seismicity, outflow temperature, and eyewitness observations. Our experiment produced a 13-month acoustic chronology of Steamboat Geyser, consisting of 23 major eruptions and weeks of precursory minor activity.

I identify common trends in Steamboat's eruptive behaviors. Typically, a major eruption starts with a short (< 1 hour) water-dominated phase, during which jetting of water reaches maximum elevations of 120m. Following the water phase, the eruption transitions to a steam-dominated phase that persists for over 12 hours post-eruption onset. Signal structure in the low infrasound bands (0.5 to 2 Hz) may be used to identify water-to-steam phase transitions in the eruption column. The long-term infrasound record is

useful for statistical analysis of eruptions and their timing. Although median major eruption intervals are about 10 days there are some outliers. Unlike other fountain-type geysers whose plumbing system is more isolated, there does not appear to be a relationship between event duration and inter-event timing.

TABLE OF CONTENTS

LIST OF TABLES

LIST OF FIGURES

## LIST OF ABBREVIATIONS

| | |
|---|---|
| YNP | Yellowstone National Park |
| NGB | Norris Geyser Basin |
| YVO | Yellowstone Volcano Observatory |
| USGS | United States Geological Survey |
| NPS | National Park Service |

# CHAPTER ONE: INTRODUCTION

Geysers are rare hydrothermal features, which intermittently erupt both liquid water and steam (White, 1967). These hydrothermal features draw millions of visitors each year to Yellowstone National Park (YNP), which contains the highest concentration of active geysers in the world (Bryan, 2018). Steamboat Geyser, a cone geyser located in the Norris Geyser Basin (NGB) of YNP, is the world's tallest active geyser with eruption column heights reaching a staggering 120 m (White et al., 1988; Reed et al., 2021). Norris, the third largest geyser basin in the park, is distinct from other basins in that it hosts uniquely sulfur-rich acidic waters and the hottest recorded water temperatures in the park (White et al., 1988; Bryan, 2018).

The two main types of geysers present at Yellowstone are fountain geysers and cone geysers. Fountain geysers are the most common type found worldwide and are defined by having an open pool of water which erupts bubbles derived from upwelling steam (Bryan, 2018). Cone geysers get their name from the form of their vent, built from a silica-rich deposit called sinter, that acts as a nozzle, emitting water and steam in a relatively high velocity jet. Both geyser types require constrictions in the subsurface plumbing so as to induce eruptions (Belousov & Belousov, 2013; Hurwitz & Manga, 2017). Cone geysers represent an example of a geologic nozzle, in which liquid water and steam are compressed at depth from the geothermal reservoir below and again at the surface from a vent structure (Kieffer, 1989). Notable cone geysers in Yellowstone

include Old Faithful, Lone Star, and Steamboat. Geyser eruptions rely on the filling and heating of water in subsurface reservoirs. These reservoirs are subject to hydrostatic pressurization as groundwater flows into the plumbing system and cavities. Rising pressures increases the boiling point of the reservoirs relative to the boiling temperature at the surface allowing reservoir water to become superheated (Hurwitz & Manga, 2017) The water continues to heat up until the local boiling point is reached, which leads to steam formation that rises vertically up the conduit and/or pushes water and steam up and out of the reservoir (Kieffer, 1989; Hurwitz et al., 2008; Dowden et al., 1991; Bryan, 2018).

Many geysers are historically long-lived features operating consistently for (at least) tens of years, yet external factors such as seismicity and climatic trends have been shown to influence geyser activity (Reed et al., 2021; Hurwitz et al., 2008; Husen et al., 2004). These external controls may affect the permeability of the conduits and the supply of water to the reservoirs, which results in induced or deactivated eruptions, and changes in the interval length between eruptions Steamboat Geyser is a dramatic example of a geysers whose historic activity is marked by periods of either subdued or consistent eruptive activity. It has only two known previous active periods (in the 1960s and 1980s) since the Park's designation in 1872 (Reed et al., 2021). The third and current active period at Steamboat Geyser began in March of 2018 with a total of 155 eruptions thus far (as of June 24, 2022). This reinvigorated stage provides the opportunity to study long-term monitoring of both major and minor eruptions.

Although Steamboat erupts more frequently during an active period, the eruptions are still separated by days to weeks. This differs from other cone geysers in YNP like Old Faithful, which erupts regularly at intervals with a bimodal distribution on the scale of hours approximately every 50 to 70 minutes (Rinehart, 1974). Steamboat's current active phase appears to show a modest seasonal modulation, with intervals slightly longer in the winter and shorter in the summer (GeyserTimes, 2022; Reed et al., 2021;). An anomalous quiescent period occurred in the summer of 2021 during which Steamboat experienced its longest intervals between eruptions with a return to semi-normal interval behavior in the fall of 2021.

Citizen scientists are also important for Steamboat observations and experienced geyser enthusiasts' reports document eruptive activity, timing, and duration estimates and contribute reports to the GeyserTimes database, a nonprofit organization "dedicated to the acquisition, preservation and dissemination of geyser-related data" (GeyserTimes, 2022). Eyewitness accounts are helpful yet only available seasonally for the months April through November due and are subject to human observational bias.

Although multiple short-term geophysical based studies of geysers have been conducted in YNP (Wu et al., 2021; Nayak et al., 2020; Johnson et al., 2013; Karlstrom et al., 2013; Vandemeulebrouck et al., 2013; Cros at al., 2011) there exists a general gap in our understanding of how geysers respond to long-term temporal changes, on the scale of weeks to months, due to a lack of extended or semi-permanent deployments. Steamboat, whose current reactivation period is only a few years long, and whose eruption statistics

is relatively small - owing to relatively sporadic eruptions - is thus particularly amenable to long term geophysical or hydrological monitoring. Long term monitoring efforts in the Norris Geyser Basin have traditionally included seismometers, temperature loggers, and stream gauges which are maintained by the USGS and National Park Service. Monitoring aimed specifically at Steamboat Geyser includes a temperature logger placed in the runoff channel implemented by the Yellowstone Volcano Observatory (USGS).

To contribute to Steamboat's continuous monitoring efforts, I deployed long-duration (13-month) infrasound sites with the objective of capturing activity, trends, and eruption statistics. I suggest that Infrasound monitoring can complement existing seismic monitoring, currently maintained by YVO at Norris, by providing data on the surface eruptive processes through sampling of atmospheric pressure waves produced by surface activity at the geyser's vent. Acoustic source monitoring is a growing discipline that complements seismic monitoring to earthquake sources. Infrasound refers to airwaves below the human-audible frequency level or under 20 Hz confined to the atmosphere; however, many natural sources, such as geysers, produce signals ranging from infrasound in the low-frequency audio band (Johnson and Ripepe, 2011). Infrasound monitoring has previously been used for studying source phenomenology of erupting volcanoes, earthquakes, avalanches, as well as nuclear test explosions (Watson et al., 2022; Johnson and Ripepe, 2011; Christie and Campus, 2009; Mutschlecner & Whitaker, 2005). Infrasound and low-frequency audio signals can propagate great distances with minimal signal attenuation relative to shorter wavelengths (Arrowsmith et al., 2010). Infrasound monitoring of volcanoes has proven useful for quantifying the style of eruptive activity,

reconstructing the eruption chronology, as well as quantifying eruption statistics over long periods of time. The same applications of infrasound sensing may prove useful in monitoring geyser activity and quantifying the surface expressions of exploding hydrothermal systems.

Previous work involving acoustic monitoring at YNP were short campaigns lasting less than one week. Johnson et al. (2013) performed a pioneering 6-day infrasound study on geysers in the Lower Geyser Basin (LGB) of YNP, finding that fountain type geysers (Great Fountain) produce abundant infrasound compared to cone type geysers (White Dome) which produced little to no detectable infrasound. Karlstrom et al. (2013) led a 4-day study chronicling the energetics and eruption dynamics of Lone Star Geyser utilizing acoustics, discharge measurements, and infrared imagery. Our study was the first implementation of long-term infrasound monitoring of a geyser, lasting 388 days. Benefits of extended monitoring periods include the ability to discern seasonal trends as well as catalog multiple events to generate robust statistics on eruptive behavior.

# CHAPTER TWO: DATA ACQUISITION AND METHODS

## Infrasound Array

We deployed two three-element infrasound arrays in the NGB located approximately 200 meters ENE and ESE from Steamboat Geyser's main vents operating from September 26th, 2020, to October 19th, 2021 (Fig. 1). Each array consisted of three InfraBSU version 2 low-frequency microphones (sensitivity of 46 μV/Pa; low-corner at ~0.1 Hz) connected to a 3-channel, 24-bit data logger (DiGOS DATA-CUBE$^3$ Type-1) recording continuously at 200 Hz.

The infraBSU version 2 infrasonic microphone is a custom-designed sensor produced at Boise State University and housed in a weather-protective PVC sheath tube to survive burial in snow and exposure to elements (Fig.1c). Operation of these sensors is similar to that outlined in Marcillo et al. (2012) and Slad and Merchant (2021). Each microphone was connected with 15m cables to the data logger and the relative position of each sensor was located using measuring tape and compass bearings (Fig.1a). The DATA-CUBE digitizer was situated in a weatherproof enclosure housing a ~150 A-hour battery bank (4 car batteries in series) designed to maintain power for at least six months when the site was inaccessible due to snow.

The units recorded continuously except for when the data loggers, which had 32 Gigabytes of internal storage, filled up on 22 March. As such there is a 3-week data gap

from March 22nd to April 17th, when we were able to visit YNP, download data, and clear memory.

## Eruption Signal Processing

Processing the infrasound data involves converting from raw DATA-CUBE format to mini-SEED (.mseed) format then importing .mseed files into Matlab. Start time of major eruptions could be easily identified with visual inspection of unfiltered waveforms and compared with the online GeyserTimes database. Geyser infrasound was more easily identified following filtering with a two-pole, high-pass Butterworth filter above 1 Hz, which reduced wind noise contamination in the data. High-pass filtered acoustic data was then used for parameter analysis, as well as time series and spectral display. All data are converted to units of pascals.

## Time lapse Imagery

Two aTLi EON time-lapse cameras were installed starting on June 1st, 2021, and both were located below and near the boardwalk adjacent to Steamboat's main vents (Fig. 1b). To maximize time duration of the camera operation I acquired imagery with a fairly low frame rate (10 seconds between frames). These cameras operated continuously and without power interruptions using an external power bank. Both cameras recorded one major eruption on July 8th, 2021, which happened during an anomalously long period of quiescence and was in fact the only eruption that occurred in the June-August timeframe. Time lapse footage also contained multiple minor eruptions preceding the major July

eruption. This imagery complements the acoustic data and provides visual confirmation of what is occurring at the surface in the eruption column.

### Other time series data: outflow temperature and seismicity

Water temperature recorded in Steamboat Geyser's main outflow channel (~40m from the south vent) provides an approximate timing estimate of when water is erupting and flowing downslope from the geyser (Fig. 1). This instrument is maintained by the USGS and serves to track minor and major eruptive activity, depending on the temperature probe's operational condition (USGS, 2022). The seismic data used in this study is sourced from the University of Utah's nodal array with a sample rate of 1000 Hz and a corner frequency of 5 Hz (Fig. 1). This seismic study aims to track seismic activity before, during, and after an active phase at Steamboat Geyser as well as model the interconnectivity of Steamboat's subsurface plumbing system (Wu et al., 2021).

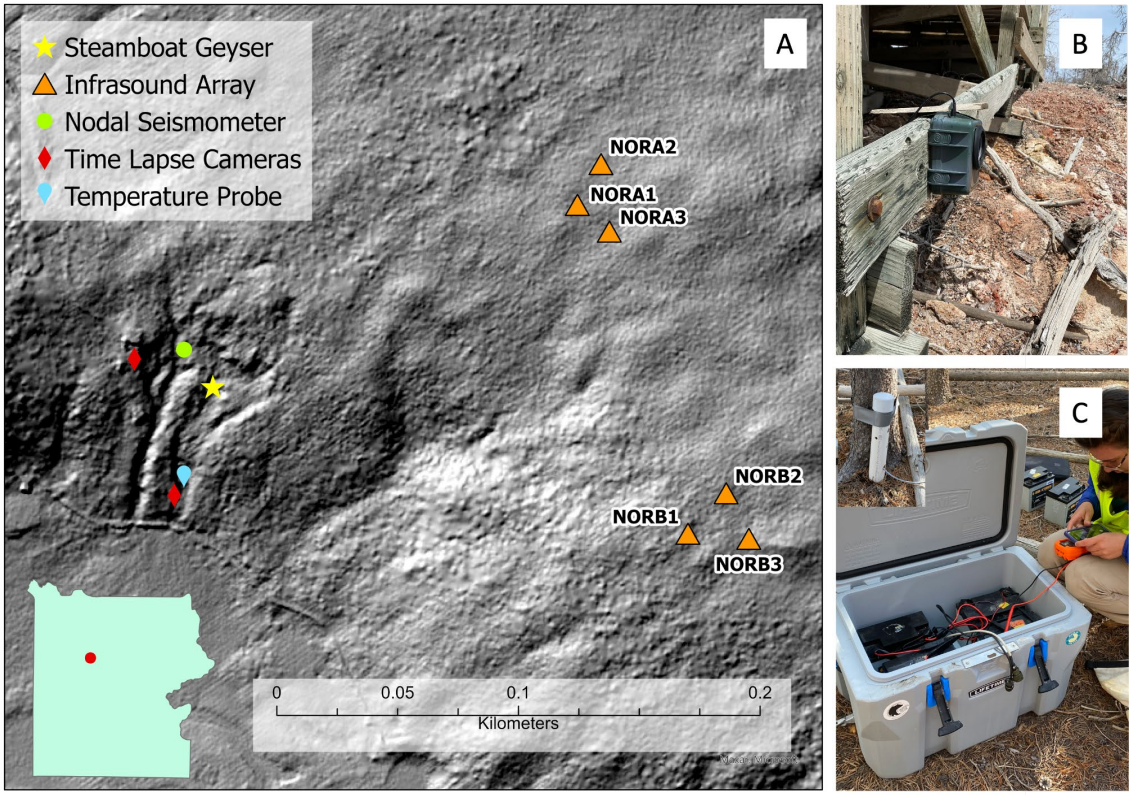


**Figure 1 Data Source Locations**

**a) Site map for the two Infrasound arrays NORA and NORB, and two time lapse cameras. Seismic node and stream outflow temperature gauge are also indicated. b) Placement of the northern time lapse camera underneath the boardwalk viewing area adjacent to Steamboat Geyser. c) Images of the NORA array, with one example microphone channel housed in protective PVC tubing (top left) and the datalogger and power supply case.**

# CHAPTER THREE: RESULTS

## Signal Overview from 13-Months of Data Acquisition

Twenty-three major eruptions were recorded during 13-months of infrasound monitoring at Steamboat Geyser. I analyzed acoustic signals to parameterize each individual major eruption. These parameters include peak-to-peak amplitudes, time-averaged power, cumulative energy, and event duration extracted from 24-hour waveforms after filtering above 1 Hz (Table 1). I also calculated the same parameters for non-eruption days to establish baseline conditions (Table 2). Peak-to-peak amplitudes of sound correspond to short-duration maximum amplitudes over the 23 eruptions. These amplitudes average 10.5 Pa, with lower mean values in the winter months and higher values in the spring, summer, and fall. I determine that the spectral content for snow covered eruptions is likely affected by snowpack attenuation of geyser signal (Keskinen et al., in prep).

Average acoustic power was calculated as the squared amplitude of filtered infrasound data (NORA channel 3) and is a proxy for sound intensity during an eruption. The cumulative acoustic energy is time-integrated acoustic power over the duration of an event. Event duration is defined as the amount of time elapsed since the impulsive eruption onset, until cumulative energy has reached 99% of its total 24-hour cumulative energy. The arbitrary cutoff is necessary because most Steamboat events taper gradually

in terms of eruption intensity and acoustic radiation. The longest duration eruption was 22.5 hours occurring on November 29th, 2020 whereas the shortest eruption duration was 7.5 hours and occurred on May 31st, 2021.

I constructed spectrograms to provide a visual representation of change in frequency over time for all major eruptions (Fig. 3). Waveforms and associated peak-to-peak amplitudes of each major eruption reveal similar signal envelope and a distinct decrease in amplitudes in winter months (Fig. 2). High frequencies (above 10 Hz) are attenuated in the spectrograms for eruptions during winter months with increased snowpack (Fig. 3). Eruptions where snow was sparse to absent show dominant frequencies between 20-60 Hz (Fig. 3). I calculated the median frequency for each eruption and used these values to also calculate the wavelength of these signals (Equation 1; Table 1).

$$\lambda = c/f_{median}$$

**Equation 1:** Wavelength (λ) in units of meters is equal to the speed of sound (c = 343 m/s, in dry air at 20 degrees Celsius) divided by the median frequency (Hz).

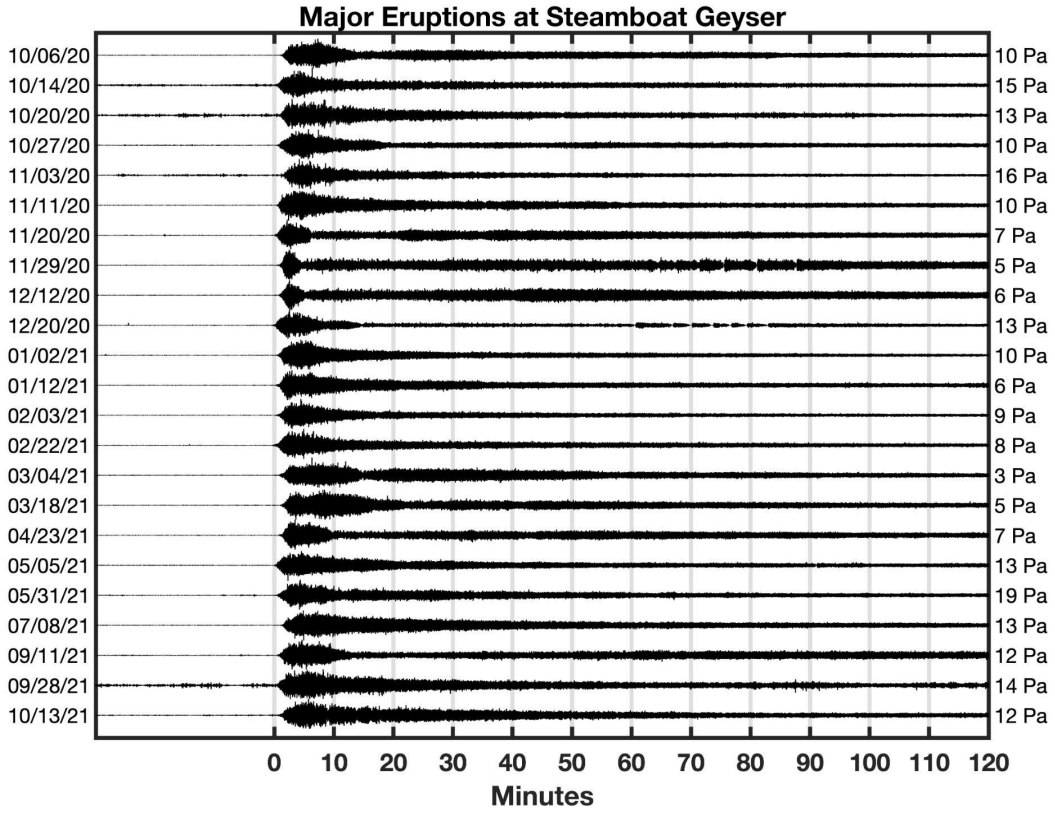


**Figure 2 Infrasound Waveforms of Major Steamboat Eruptions**

**The first two hours of aligned waveforms from 23 major Steamboat eruptions, acquired from microphone channel 3 of the NORA array and high pass filtered above 1 Hz. Corresponding peak-to-peak amplitudes are listed on the right and date of eruption is provided on the left.**

**Table 1 Acoustic Parameters derived from sensor 3 at array NORA for major geyser eruptions at Steamboat.**

| **Major Eruption Date** | **Eruption Onset (UTC)** | Event Duration Filtered above 1 Hz (hrs) | Peak to peak amplitudes Filtered above 1 Hz (Pa) | Average Power Filtered above 1 Hz (Pa^2) | Cumulative Energy ($Pa^2S$) for 24hrs from Avg Power filtered above 1 Hz | Snow Depth Canyon SNOTEL Site (cm) | Median Frequency (Mean from 1st hour post eruption onset) | Wavelength of Median Frequency (m) |
|---|---|---|---|---|---|---|---|---|
| **10/13/2021** | 18:44 | 14.11 | 12.3 | 0.0273 | 2354.8 | 7.62 | 32.79 | 10.5 |
| **9/28/2021** | 19:27 | 10.76 | 13.5 | 0.0354 | 3055.6 | 0 | 35.43 | 9.7 |
| **9/11/2021** | 12:38 | 13.72 | 11.9 | 0.0291 | 2512.7 | 0 | 35.26 | 9.7 |
| **7/8/2021** | 12:33 | 12.99 | 12.8 | 0.0354 | 3061.3 | 0 | 37.38 | 9.2 |
| **05/31/21** | 17:43 | 7.54 | 19.2 | 0.0458 | 3953.8 | 0 | 38.55 | 8.9 |
| ***5/5/2021** | 06:02 | 17.99 | 13.5 | 0.0245 | 2116.8 | 58.42 | 36.96 | 9.3 |
| ***4/23/2021** | 14:56 | 13.74 | 6.6 | 0.0068 | 584.5 | 88.9 | 25.52 | 13.4 |
| ***3/18/2021** | 09:43 | 11.67 | 4.5 | 0.0046 | 399.9 | 101.6 | 13.58 | 25.3 |
| ***3/4/2021** | 01:50 | 18.23 | 2.9 | 0.0020 | 177.1 | 106.68 | 12.87 | 26.7 |
| ***2/22/2021** | 02:20 | 19.37 | 7.9 | 0.0037 | 320.8 | 109.22 | 10.81 | 31.7 |
| ***2/3/2021** | 09:01 | 18.83 | 8.9 | 0.0077 | 667.5 | 83.82 | 17.84 | 19.2 |
| ***1/12/2021** | 15:58 | 17.81 | 6.1 | 0.0059 | 509.39 | 50.8 | 16.93 | 20.3 |
| ***1/3/2021** | 00:00 | 17.71 | 14.4 | 0.0109 | 937.9 | 48.26 | 19.71 | 17.4 |
| ***12/20/2020** | 19:14 | 16.23 | 12.7 | 0.0099 | 858.2 | 43.18 | 17.00 | 20.2 |
| ***12/11/2020** | 03:41 | 16.59 | 5.9 | 0.0081 | 700.8 | 25.4 | 21.54 | 15.9 |
| ***11/29/2020** | 21:36 | 22.49 | 5.3 | 0.0071 | 616.5 | 15.24 | 23.15 | 14.8 |
| ***11/20/2020** | 17:12 | 18.27 | 7.2 | 0.0082 | 709.3 | 20.32 | 27.37 | 12.5 |
| ***11/11/2020** | 13:05 | 13.68 | 10.2 | 0.0173 | 1493.4 | 10.16 | 33.00 | 10.4 |
| ***11/3/2020** | 20:32 | 11.64 | 16.0 | 0.0225 | 1941.7 | 5.08 | 35.34 | 9.7 |
| ***10/27/2020** | 08:42 | 13.38 | 10.4 | 0.0124 | 1067.9 | 5.08 | 27.04 | 12.7 |
| ***10/20/2020** | 04:40 | 22.26 | 12.8 | 0.0254 | 2191.0 | 5.08 | 36.80 | 9.3 |
| **10/14/2020** | 07:11 | 18.12 | 15.5 | 0.0359 | 3101.4 | 0 | 36.53 | 9.4 |

| **Major Eruption Date** | **Eruption Onset (UTC)** | Event Duration Filtered above 1 Hz (hrs) | Peak to peak amplitudes Filtered above 1 Hz (Pa) | Average Power Filtered above 1 Hz (Pa^2) | Cumulative Energy ($Pa^2S$) for 24hrs from Avg Power filtered above 1 Hz | Snow Depth Canyon SNOTEL Site (cm) | Median Frequency (Mean from 1st hour post eruption onset) | Wavelength of Median Frequency (m) |
|---|---|---|---|---|---|---|---|---|
| **10/13/2021** | 18:44 | 14.11 | 12.3 | 0.0273 | 2354.8 | 7.62 | 32.79 | 10.5 |
| **10/6/2020** | 03:04 | 19.76 | 10.1 | 0.0156 | 1350.7 | 0 | 37.88 | 9.1 |

*Dates with snowpack sourced from Canyon SNOTEL site. Subsequent data in the table is subject to influence of snowpack attenuation. Dates with no star but with Canyon snow depth coincided with site visits which confirmed no snow presence.

**Table 2 Acoustic Parameters derived from sensor 3 at array NORA for non-eruption days.**

| Date | Peak to peak amplitudes (Pa) | Average Power ($Pa^2$) | Cumulative Energy ($Pa^2S$) for 24hrs | Median Frequency (Hz) | Wavelength of Median Frequency (m) |
|---|---|---|---|---|---|
| 10/15/21 | 3 | 0.002 | 179 | 3 | 114.3 |
| 9/30/21 | 4 | 0 | 147 | 10 | 34.3 |
| 9/13/21 | 2 | 0.001 | 257 | 6 | 57.2 |
| 7/10/21 | 2 | 0.001 | 475 | 10 | 34.3 |
| 6/2/21 | 2 | 0.001 | 103 | 10 | 34.3 |
| 5/7/21 | 6 | 0.009 | 171 | 4 | 85.8 |
| 4/24/21 | 1 | 0 | 28 | 7 | 49 |
| 3/19/21 | 0 | 0 | 13 | 4 | 85.8 |
| 3/5/21 | 0 | 0 | 7 | 5 | 68.6 |
| 2/24/21 | 2 | 0 | 11 | 5 | 68.6 |
| 2/4/21 | 2 | 0 | 31 | 6 | 57.2 |
| 1/13/21 | 7 | 0.001 | 62 | 5 | 68.6 |
| 1/6/21 | 4 | 0 | 9 | 6 | 57.2 |
| 12/22/20 | 6 | 0.001 | 77 | 4 | 85.8 |
| 12/13/20 | 2 | 0.001 | 49 | 4 | 85.8 |
| 11/30/20 | 3 | 0.004 | 316 | 12 | 28.6 |
| 11/21/20 | 2 | 0.002 | 203 | 9 | 38.1 |
| 11/12/20 | 2 | 0.001 | 119 | 5 | 68.6 |
| 11/5/20 | 4 | 0.004 | 345 | 4 | 85.8 |
| 10/28/20 | 1 | 0 | 18 | 5 | 68.6 |
| 10/21/20 | 6 | 0.009 | 743 | 2 | 171.5 |
| 10/15/20 | 3 | 0.003 | 214 | 3 | 114.3 |
| 10/7/20 | 2 | 0.001 | 95 | 6 | 57.2 |

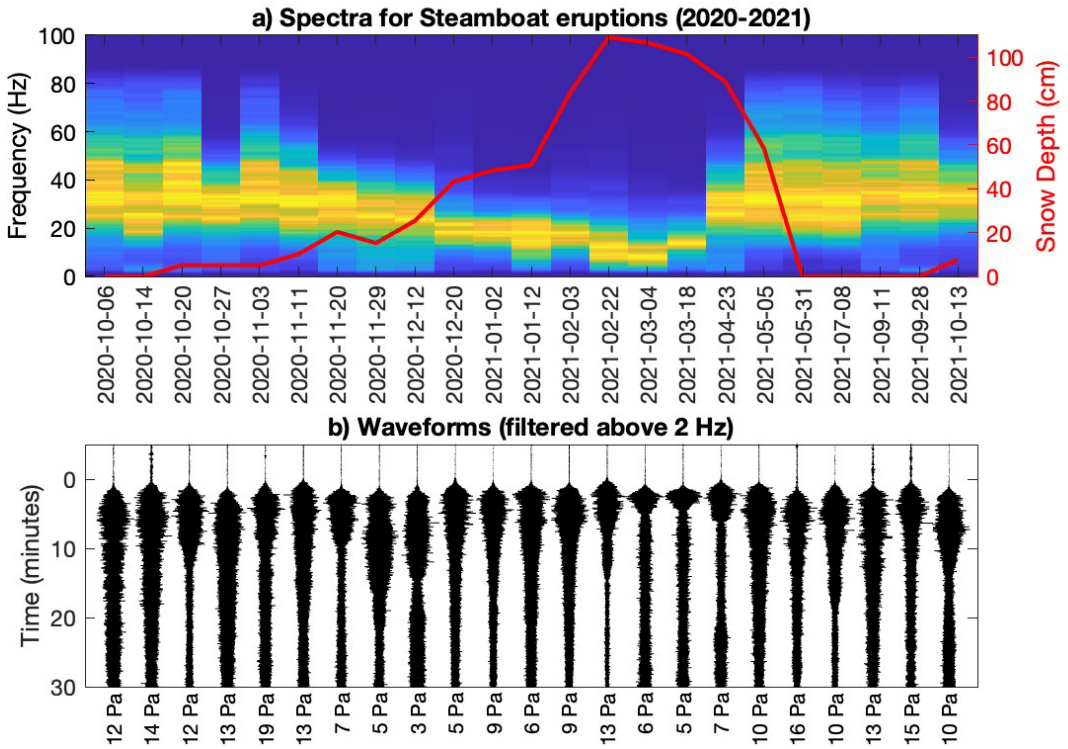


**Figure 3 Comparison of Snow Depth to Infrasound Spectra and Waveforms**

**Infrasound amplitude spectra (a) and waveforms (b) for the 23 Steamboat major eruptions recorded between Oct 2020 - 2021. Spectra are normalized to peak values in each column. Each event represents the first 30 minutes of the event filtered above 2 Hz. Snow depths (red line in panel a) are from the Canyon SNOTEL site.**

## Anatomy of a single eruption on 8 July 2021

I analyzed in detail an example major eruption event occurring on 8 July 2021 to better understand the relationship between eruptive activity and acoustic radiation. This specific eruption, with acoustic duration of 12.99 hours (Table 1), was chosen because it was the only event to occur in the summer of 2021, free from snowpack attenuating effects and recorded by multiple data streams including infrasound, seismic, time-lapse imagery, and outflow water temperature as well as eyewitness accounts. The waveform

and spectrogram reveal characteristic behaviors of all Steamboat eruptions, which begin with high amplitudes (associated with the most violent part of the Steamboat major eruptions), which diminish exponentially during the first few hours before decaying more gradually until the end of the event. Steamboat acoustic radiation is concentrated between 1 and 80 Hz, with median frequencies (calculated from the first hour of each eruption) ranging from a high of 39 Hz to a low of 11 Hz (Table 1). Median frequencies were lowest in months with snowpack present and highest in months with no snow (Table 1). Between about 17:00 UTC and 03:00 UTC low frequency energy (1-5 Hz) is apparent, but I suspect this is noise and non-geyser signal because it is poorly correlated across the array elements. The spectrogram also shows a few distinct bands that endure for over 12 hours at 25 Hz and 35 Hz. Because they are not evident prior to the onset of the Steamboat eruption I consider them to be related to the eruption.

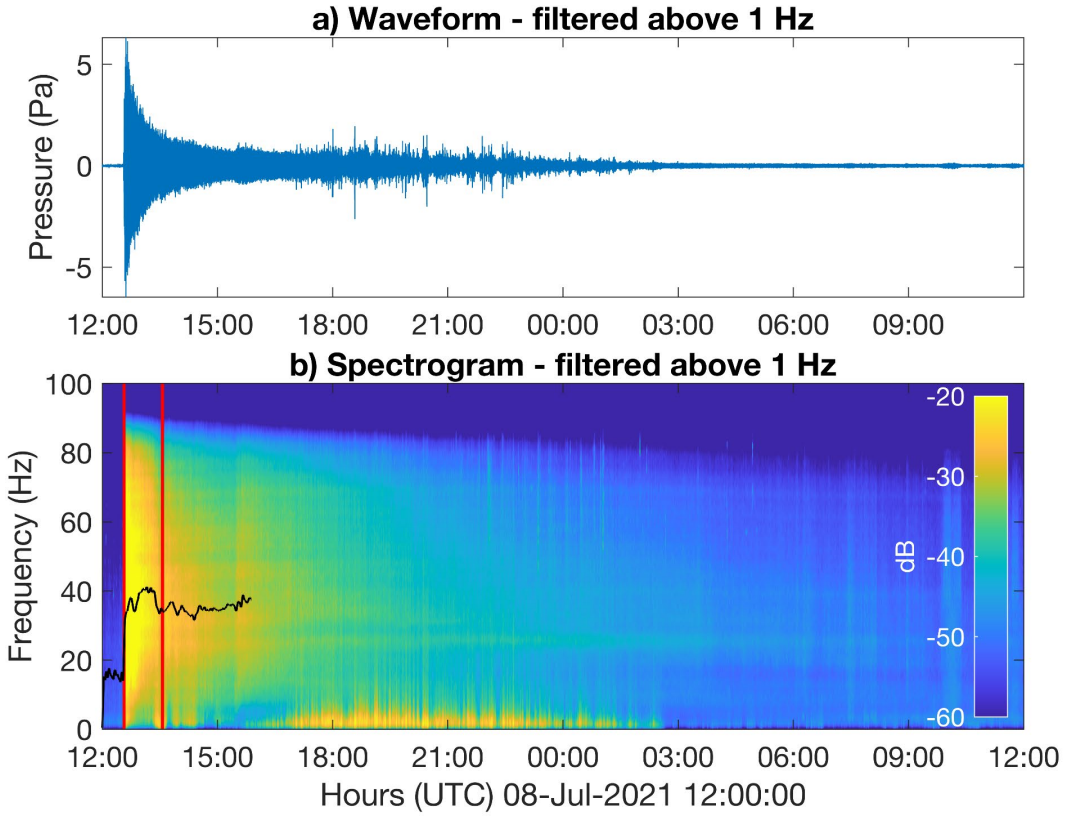


**Figure 4 Major Eruption Infrasound Waveform and Spectra**

**Waveform (a) and spectrogram (b) for the 8 July 2021 eruption. A waveform represents the change in acoustic amplitude (Pa) over the course of the eruption. The spectrogram shows the change in frequency over time with the power in decibels of a sound source. The black line is the median frequency, cropped for clarity. Red lines bracket the 1-hour period from which the average median frequency was derived (Table 1).**

The initial few hours of Steamboat eruptions are the most violent and dynamic in terms of evolving eruption characteristics and I examined the band-filtered acoustic recordings to correlate eruptive behavior with acoustic radiation. Filtering and displaying the acoustic signal into distinct frequency ranges (Figure 5) reveals structure in lower frequency bands (0.5 to 2 Hz and 2 to 8 Hz) that is not evident in the more powerful 8-64

Hz band or in the seismic data, which are also band-filtered. The seismic data were filtered with an 11-sample median filter to remove glitches in the signal.

Visual observations from William Beverly, a contributor to GeyserTimes, are particularly useful for understanding fluctuations in the low-frequency acoustic envelope in the infrasound band, which shows an enhanced pulse of energy between 50 and 70 minutes after the eruption onset (Fig. 5). This corresponds to a reported phase transitions in the eruption column from water to steam, and to start/stop sequences referred to as ‘choking’ by W. Beverly (GeyserTimes and pers. comm.).

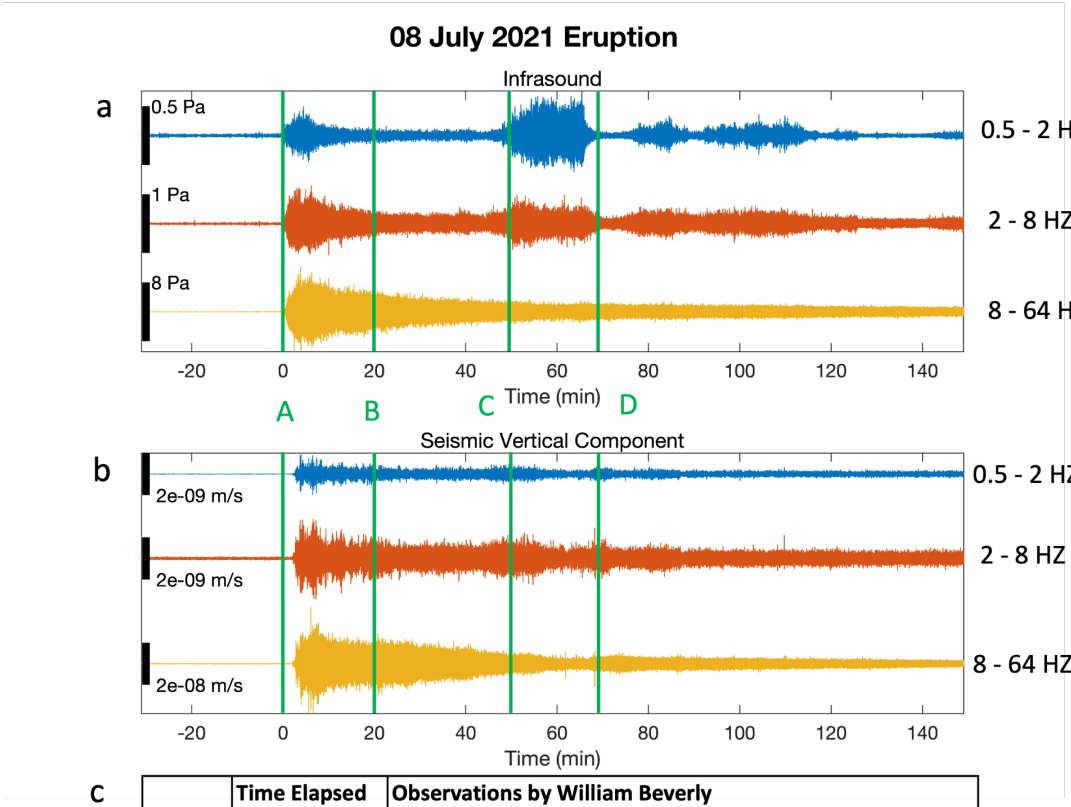


c

| | Time Elapsed | Observations by William Beverly |
|---|---|---|
| A | 0 min | The eruption starts, both vents are ejecting liquid water. |
| B | 20 min | The North Vent begins steam phase. |
| C-D | 50-68 min | Both vents return to water phase (no choking occurs). |
| D | 68 min | Both vents begin full steam phase. |

**Figure 5 Frequency Dependent Infrasound and Seismic Waveform Comparison**

**(a) 2.5 hours of acoustic signal for the 08 July 2021 eruption filtered into 3 frequency ranges from low infrasound to low audible. (b) Corresponding seismic signal from the start of the 08 July 2021 eruption filtered into 3 frequency ranges. (c) Timing of significant events of interest are indicated with letters and lines corresponding to first-hand observations made during the eruption**

## Precursors to a major event

Minor geyser activity at Steamboat, defined as episodic water eruptions jetting 3 to 15 m high, is a common feature at Steamboat and is anecdotally associated with the days leading up to major eruptions (White et al., 1988). Tracking minor geyser activity at

Steamboat Geyser is possible with acoustic monitoring. Upticks in minor geyser activity precede a major eruption by upwards of a week and can thus be used to constrain timing before a major geyser eruption. The current method for tracking minor activity, or short bursts of hot water, is through a temperature logger located in the main outflow channel southwest of the main vents. When hot water erupts from the vents during a minor event, it flows downslope and raises the temperature in the channel above ambient air reading. When water is not flowing over the temperature sensor, readings are interpreted as ambient air temperature. In addition to major events, the infrasound data also has the ability to track Steamboat's minor activity.

Cross correlation analysis of infrasound signals using multiple elements of an acoustic array is effective to verify whether acoustic signal is present and originates from Steamboat Geyser or a different source location (Fig. 6a). I analyzed long-term acoustic records from NORA to identify whether coherent sound comes from the WSW, the direction of Steamboat. During periods of relatively low wind speed each night it is possible to identify the presence of minor geyser activity. Normalized cross correlation values suggest signals arrive from WSW, the direction of Steamboat. These cross correlations are calculated hourly and used as a proxy to identify the occurrence of minor Steamboat activity leading up to and following the July 8 Steamboat major event. It is notable that cross-correlation values cycle from low to high during a 24-hour period due to the fact that afternoon wind noise contaminates the recordings. Even so, gradually increasing cross correlation amplitudes are evident starting around June 10 and indicate increasing amounts of minor activity. After the July 8 major event, minor activity

appears to taper for a couple of days and then returns to low amplitudes. Not surprisingly, the day with the highest cross correlation value is the eruption day on 8 July 2021, with an average value of 0.6. Days preceding the eruption have varying scores of 0.26 to 0.36 and increase in the lead-up to the major event.

Comparing the infrasound detection proxy with stream outflow temperatures (Fig 6b) provides a long-term record of the precursor to a major event on July 8th.
The temperature probe, situated in the outflow channel beneath Steamboat, can be used to identify when a major or minor eruption occurs as water is ejected then flows downslope over the temperature probe. Elevated water temperatures correspond to Steamboat-derived water sources, which peak during a major eruption. Obvious diurnal fluctuations correspond to ambient air temperatures.

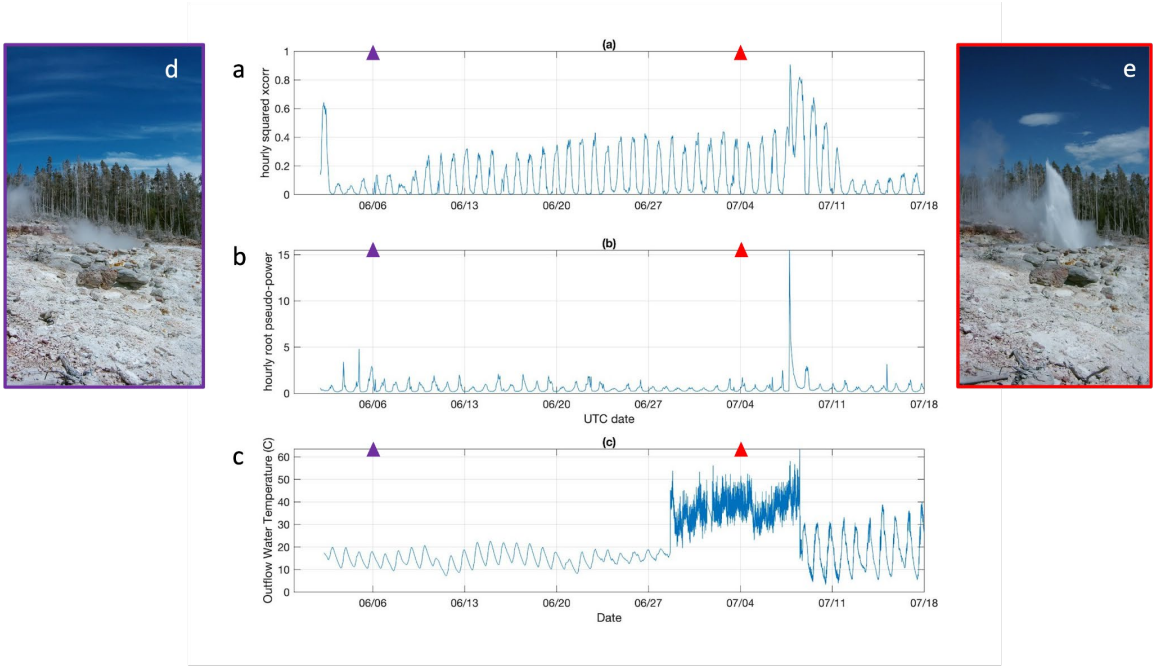


**Figure 6 Six-week chronology of Steamboat activity**

**(a) Normalized cross-cross-correlation is computed at hourly intervals. Low values correspond to daily periods of high wind occurring every day in the afternoon. (b) Square root of pseudo-power (Pa) is also computed during hourly intervals. The July 8 event is evident in both (a) and (b). (c) Outflow temperatures measured in the channel below Steamboat. The probe was covered in outflow water between approximately June 29 and July 9. Daily cycles occurring at beginning and end of time series are evident and correspond to conditions when temperature probes are exposed to the atmosphere. The onset of the major event on July 8th is indicated. Details of 4.5 hours of this major eruption is provided in Fig. 7. (d) An image from the time lapse record on June 6, 2021, showing typical quiescent behavior post-eruption (recent eruption occurred on May 31, 2021), indicated by the purple triangle in the time series. (e) An image of minor activity from July 4, 2021, time lapse record indicated by the red triangle in the time series. Water jetting as shown in this still is frequent leading up to a major eruption.**

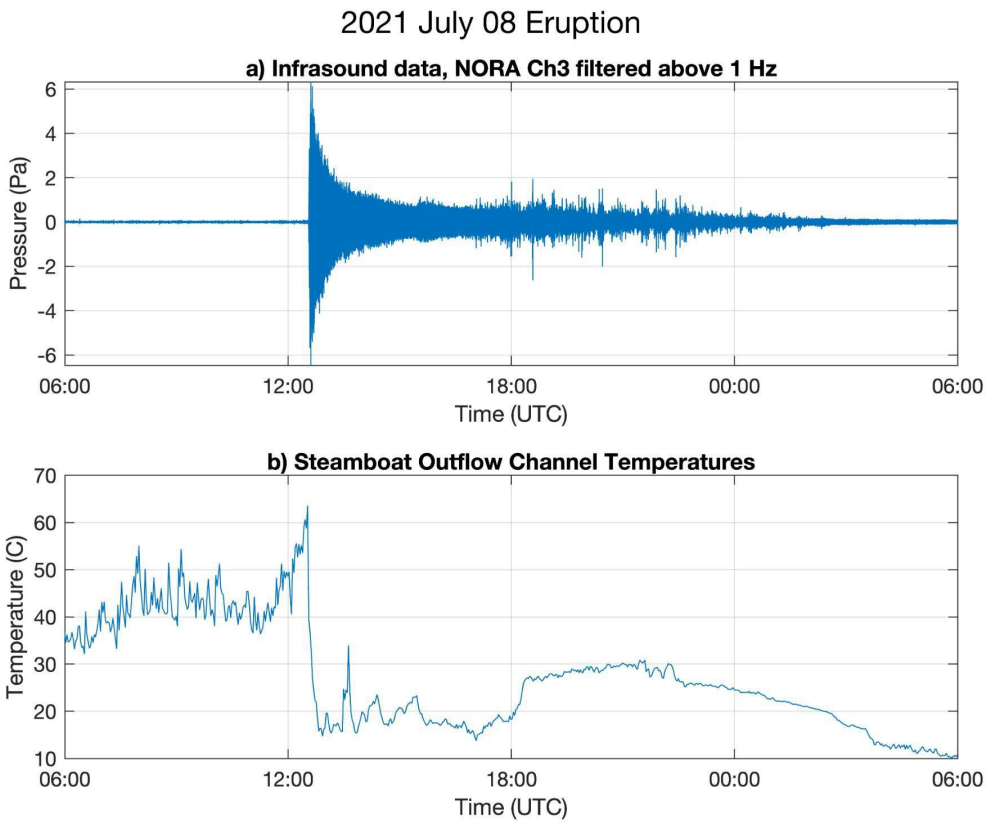


**Figure 7 24-hour detail of the 8 July 2021 Steamboat eruption**

**(a) Infrasound waveform from NORA array channel 3 with eruption onset occurring after 12:33 UTC and (b) corresponding outflow water temperature data.**

# CHAPTER FOUR: DISCUSSION

## Long-Term Infrasound Monitoring and Eruption Statistics

Using an ensemble suite of 23 major eruptions, I can quantify Steamboat Geyser's surface eruption dynamics using infrasound-derived parameters including the timing, duration, power, and relationships between minor and major activity. This 13-month infrasound-focused study is one of the first long-term continuous infrasound monitoring campaigns focused primarily on a geyser in YNP.

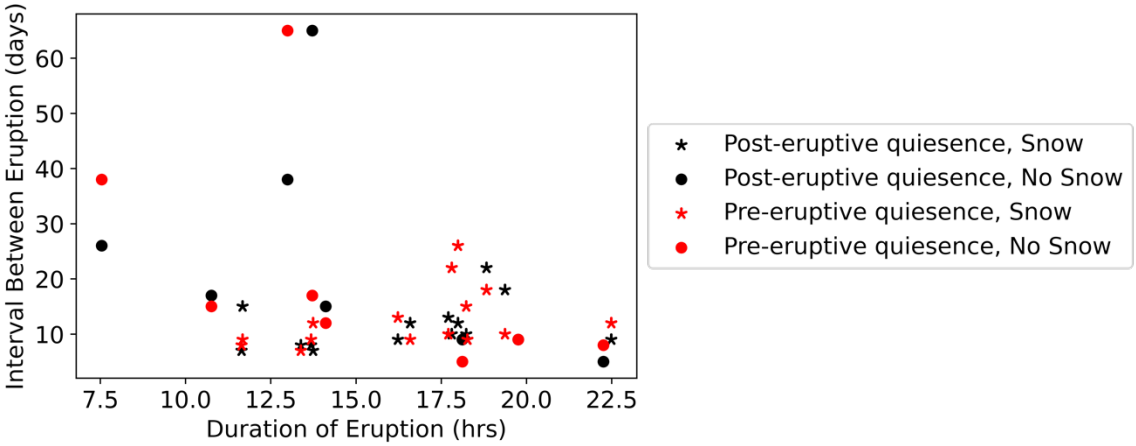


**Figure 8 Eruption Duration Compared to Interval Between Events**

**Scatter plot comparing durations of eruptions to intervals between eruptions for the October 2020 - October 2021 monitoring period. Eruption durations were calculated using channel 3 of the NORA array, high pass filtered above 1 Hz (Table 1). Inter-event intervals are shown both for time in days following (black color) and preceding (red color) a major eruption. Inferred snow-covered and non-snow-covered data are indicated with different symbols.**

As an example, long-term monitoring can be used to identify a relationship between repose duration (between major events) and eruption durations. Previous infrasound studies at Great Fountain Geyser (in Middle Geyser Basin at YNP) revealed that longer intervals between eruptions were associated with longer duration eruptions (Bryan, 2018; Johnson et al., 2013). I searched for relationships between eruption duration repose at Steamboat Geyser corresponding to both pre-eruption and post-eruption repose intervals, defined as the time between end of one major eruption and beginning of next eruption. Statistics for snow-free (summer) and snow-covered (winter) were separated to try to assess whether seasonal variables were significant (Fig. 8). Because no direct relationships were evident with either snow covered or snow free conditions, I conclude that recharge time is not directly related to volume of water erupted using eruption duration as a proxy for outflow. Regular and predictable eruption behavior of geysers such as Old Faithful and Great Fountain can be attributed to their large and deep hydrothermal plumbing systems which are insulated from the effects of surface water (Hurwitz & Manga, 2017). Geographically isolated geysers are more regular since eruptions influence the eruption intervals of proximal geysers (Fagan et al., 2022; Hurwitz & Manga, 2017). Cone-type geysers display the greatest influence over other geysers' eruption intervals but also remain the most insulated from extra-geyser effects (Fagan et al., 2022). Although deep and large systems promote regularity of geyser eruptions and Steamboat is relatively isolated from other major cone geysers, I find no obvious relationship between these parameters. I suspect that exchange of function at Steamboat, meaning the interplay with Cistern Pool, may explain the irregularity of Steamboat (Wu et al., 2021). In addition to Steamboat’s highly complex

hydrologic system, it hosts the deepest reservoir of any active geyser which correlates to having the tallest eruptions (Wu et al., 2021; Reed et al., 2021). With a system as large, deep, and complex as Steamboat, irregular eruption intervals are in line with expectations based on both field and laboratory models of geysers (Wu et al., 2021; Hurwitz & Manga, 2017; Adelstein et al., 2014; Davis, 2012). Benefits of long-term acoustic monitoring may include the identification of potential seasonal impacts (i.e., snowpack) on eruptive periodicity or eruptive style.

During the winter months, I observe a significant decrease in recorded infrasound energetics and an absence of higher frequencies over 25 Hz (Table 1, Fig. 3). One hypothesis is that eruption mechanisms are fundamentally different during cold periods and/or when Steamboat vicinity and vent is mantled with a snowpack. Upon consideration, however, it is more plausible that snowpack-derived signal attenuation at the receiver is likely, and this results in a low pass filter (Iwase et al., 1997; Johnson; 1982; Fig. 3; Table 1). Although there is no snow depth data available at NGB (elev. 2298m), a comparison of infrasound data with the closest snowpack data from either Old Faithful (29 km SW), which has a similar elevation (2296m) or the Canyon SNOTEL site (15 km E, elev 2430m) show that Steamboat signals are attenuated when snowpack is likely covering sensors. I observe that the early winter season (October - mid December) and presumably thinner snowpack coverage yields minimal attenuation effects.

## Tracking Geyser Activity

Tracking major and minor eruptive activity at Steamboat Geyser is possible using infrasound-based sensing. Tracking minor activity sourced at Steamboat is best

accomplished using cross-correlation array analysis (Figure 6) to identify subtle infrasound signals hidden in noisy (windy) conditions. Often it is easier to identify geyser activity at night during periods of low wind. During the daytime wind noise tends to be higher and it inhibits detection capabilities of infrasound. Sometimes minor activity recorded with the time-lapse cameras are not evident at NORA and NORB. These infrasound-derived observations of minor activity support the hypothesis by Reed et al. (2021) that increasing minor activity precedes major eruptions (Reed et al., 2021). Tracking of Steamboat's minor activity might then be used to develop probabilistic models for forecasting the next major eruption since eruptions do not follow regular predictable intervals.

Figure 6 shows a ~20-day chronology summarizing how increasing infrasound detection for minor activity precedes a single major event on July 8. Time-lapse imagery during this period validates our interpretation of minor activity or water jetting. Outflow temperature data (Figure 6a) also confirms the presence of increased water outflux. Infrasound observations complement the water temperature logger data because it reflects vigorous eruptive activity. I speculate that passive water outflow, which may be observable in stream outflow values, is not readily detected with acoustic tools. The temperature sensors are a valuable monitoring tool, subject to both burial and repositioning during vigorous water outflow. The infrasound data provides a long-term record that relates to eruptive vigor and eruption dynamics.

**Infrasound as a tool to infer eruption dynamics**

Filtering the acoustic waveforms into specific frequency bands reveals a signal structure that aligns with observed water-to-steam phase transitions (Fig. 5). Eyewitness observations are especially important for the interpretation of the infrasound sequence. The apparent signal structure could relate to the re-emergence of a liquid water phase before both the North and South vents enter a full steam phase, approximately 70 minutes post-eruption onset. The signal structure is not as apparent in the seismic waveforms, suggesting that this phase transition is dominantly air coupled rather than ground coupled (Fig. 5). Choked flow is a term used by geyser observers, which refers to the temporary shutting off of a major eruption due to surface water flow over the two vents. Choking is apparent at Steamboat Geyser and for the July 8 eruption it occurs at 50 minutes post-eruption onset (Fig. 5). Water ejected during an eruption appears to accumulate upslope of both vents, and the return flow downslope passes over both erupting vents temporarily shutting off an eruption. This activity is likely to affect how the style of eruption varies between events. I suggest that choked flow might be common in the events occurring on November 29 and December 20, whose infrasound manifests more pulsing behavior (Fig. 1).

Sound produced by geysers exhibits qualities that are comparable to volcanic sounds, which presents the opportunity for geyser eruptions to act as potential analogs to better understand volcanic eruptions (Johnson et al., 2013). Thus, geyser eruptions allow for a window into eruptive column dynamics that are otherwise rare in nature and difficult to replicate in a manufactured setting (Karlstrom et al., 2013; Kedar et al. 1996;

Kieffer 1989). Geysers and volcanoes both have explosive eruptions that produce infrasound, but there are fundamental differences in their systems. Major jetting eruptions of geysers are caused by sudden hydrostatic pressure release due to boiling in both the conduit and chamber which repeats cyclically, on the scale of hours to days to weeks depending on multiple factors related to the geometry and recharge rate of the feature's hydrothermal reservoir (Adelstein et al., 2014). Volcanic jetting exists in different forms and scales, from fumaroles to hazardous plinian eruption columns. Both geyser and volcanic eruptions produce acoustic signals that span the infrasound and audible frequency ranges with behaviors comparable to jet engine produced noise (McKee et al., 2016; Kieffer 1989).

## Final Comments

The collected acoustic data are a subset of Steamboat's 4-year active period, including both typical and anomalous eruption-interval behavior. The anomalous behavior in the data set occurred during the summer of 2021 in which two long intervals (37 and 65 days) between eruptions at Steamboat persisted during what usually is a period of short intervals (3 to 5 days) between eruptions (Geyser Times, 2022). Looking back at the previous summers between the months of May-August, Steamboat erupted 22, 20, and 12 times in 2020, 2019, and 2018 respectively. This is significantly more frequent than the anomalous May-August 2021 period when there were only two Steamboat eruptions.

Anomalous behavior in geysers might be an indicator of changing conditions or hazards in geyser basins. With the Summer of 2021 experiencing the longest intervals between eruptions since the beginning of the 2018 active phase, initial inferences pointed to this change as the first sign of the decline of Steamboat's active period. The Norris Geyser Basin experiences yearly 'disturbances' also known as the annual temperature phenomenon in which hydrothermal features endure changes in water temperature, chemistry, increased water and gas discharge, and turbidity (Fournier et al., 1991). These disturbances occur between late summer and early fall, during which changes in geyser eruptive patterns occur as a result of varying temperature and pressure conditions caused by the annual disturbance, a possible reason for Steamboat Geyser's infrequent eruptive behavior in the summer of 2021 (Fournier et al., 1991).

Hydrothermal explosions are a possible hazard during these disturbance periods and have the potential to create or destroy geysers (Fournier et al., 1991). A well-witnessed paroxysm of a geyser in NGB, for example, occurred at Porkchop Geyser on Sept. 5th, 1989. Porkchop Geyser's eruption activity transitioned from an occasionally erupting fountain geyser to an audible "perpetual spouter" out of a drained pool which persisted up until the column rose 20-30m just before the hydrothermal explosion blew out the feature entirely, leaving a crater behind (Fournier et al., 1991). Hydrothermal explosions are a more probable hazard at Yellowstone National Park in the short term rather than an explosive volcanic eruption (USGS, 2015; Morgan et al., 2009). The mechanism driving this type of explosion is a rapid phase change from liquid water to steam potentially due to a sharp drop in pressure in the subsurface hydrothermal

reservoirs (Morgan et al., 2009; Muffler et al., 1971). The sudden onset of a volume increase of the molecules from liquid to gas associated with this phase change causes the reservoir to expand upward and outward, ejecting water, steam, and rocks in the process (Morgan et al., 2009; Muffler et al., 1971). Understanding where these reservoirs exist and the interconnectivity between features could aid in hazard assessments for popular geyser basins throughout Yellowstone National Park. Infrasound monitoring, which is continuous, may be valuable for quantifying long-term trends in activity.

This project focused on the infrasound and low audible frequency ranges of Steamboat Geyser eruptions. It is important to note that this does not represent the full spectral range of this geyser's eruptions. Collecting and analyzing the higher acoustic frequencies may provide more comprehensive statistics and offer a clearer answer to liquid to steam phase change dynamics. For the scope of this study, the 200 Hz sample rate was chosen to focus on infrasound and low audible frequencies as well as to permit the data collection to run for multiple months without site maintenance. Wind noise is a persistent issue in acoustic monitoring and efforts to correlate daytime infrasound signal to visible time-lapse imagery were hampered due to consistent daytime winds. Placing the arrays closer to the source or adding more microphones could be a mitigation measure for future infrasound deployments. Performing a methodical site selection using wind probability could also aid in a less-contaminated record. These measures would add clarity to infrasound's ability to track minor geyser activity.

# CHAPTER FIVE: CONCLUSION

Infrasound monitoring can serve as a useful and reliable and non-intrusive tool to track geyser activity and quantify eruptive statistics. Using infrasound-derived eruption statistics, Steamboat Geyser, a cone geyser, displays no direct relationship between eruption duration and the interval between eruptions, which differs from previous infrasound studies on fountain geysers in YNP. Future implementations of long-term infrasound monitoring should include localized snow depth data collection to further understand the implications of signal attenuation due to snowpack. Many geyser researchers assert the need for long-term continuous monitoring of these hydrothermal features to capture comprehensive and objective quantitative records of durations and intervals between eruptions (Reed et al., 2021; Hurwitz & Manga, 2017; Johnson et al., 2013). This study is the first of its kind to prove the feasibility and effectiveness of infrasound as a long-term surface process focused monitoring tool. The ability to discern variations in eruption dynamics, such as phase transitions between steam in water using time series data, provides a novel method to quantify stages of hydrothermal eruptive processes. Multidisciplinary monitoring using a suite of tools is advantageous to fully capture the scope of a Steamboat Geyser eruption sequence. Each data stream (infrasound, seismic, temperature outflow, time-lapse, eyewitness) lends complementary insights into different aspects of the eruptive activity.

# REFERENCES

Adelstein, E., Tran, A., Saez, C. M., Shteinberg, A., & Manga, M. (2014). Geyser preplay and eruption in a laboratory model with a bubble trap. Journal of Volcanology and Geothermal Research, 285, 129–135. https://doi.org/10.1016/j.jvolgeores.2014.08.005

Arrowsmith, S. J., Johnson, J. B., Drob, D. P., & Hedlin, M. A. H. (2010). The seismoacoustic wavefield: A new paradigm in studying geophysical phenomena. *Reviews of Geophysics*, *48*(4), 1–23. https://doi.org/10.1029/2010RG000335

Belousov, A., Belousova, M., & Nechayev, A. (2013). Video observations inside conduits of erupting geysers in Kamchatka, Russia, and their geological framework: Implications for the geyser mechanism. *Geology*, *41*(4), 387–390. https://doi.org/10.1130/G33366.1

Bryan, T. Scott. (2018). *The Geysers of Yellowstone*. 5th ed. University Press of Colorado.

Christie, D. R., & Campus, P. (2009). The IMS Infrasound Network: Design and Establishment of Infrasound Stations. In A. le Pichon, E. Blanc, & A. Hauchecorne (Eds.), *Infrasound Monitoring for Atmospheric Studies* (pp. 29–75). Springer Netherlands. https://doi.org/10.1007/978-1-4020-9508-5_2

Cros, E., Roux, P., Vandemeulebrouck, J., & Kedar, S. (2011). Locating hydrothermal acoustic sources at Old Faithful Geyser using Matched Field Processing. Geophysical Journal International, 187(1), 385–393. https://doi.org/10.1111/j.1365-246X.2011.05147.x

Davis, B. (2012). Observations of Small Model Geysers with Variable Plumbing. In *The GOSA Transactions* | (Vol. 12).

Dowden, J., Kapadia, P., Brown, G., & Rymer, H. (1991). Dynamics of a geyser eruption. *Journal of Geophysical Research*, *96*(B11), 59–71. https://doi.org/10.1029/91jb01584

Fagan, W. F., Swain, A., Banerjee, A., Ranade, H., Thompson, P., Staniczenko, P. P. A., et al. (2022). Quantifying interdependencies in geyser eruptions at the Upper Geyser Basin, Yellowstone National Park. Journal of Geophysical Research: Solid Earth, 127, e2021JB023749. https://doi. org/10.1029/2021JB023749

Fournier, R. O., Thompson, J. M., Cunningham, C. G., & Hutchinson, R. A. (1991). Conditions leading to a recent small hydrothermal explosion at Yellowstone National Park. *Geological Society of America Bulletin*, *103*(8), 1114–1120. https://doi.org/10.1130/0016-7606(1991)103<1114:CLTARS>2.3.CO;2

Geyser Times. (2022). *Steamboat Geyser Major Eruption Chronology*. Retrieved August 2022, from https://geysertimes.org/geyser.php?id=Steamboat

Hurwitz, S., Kumar, A., Taylor, R., & Heasler, H. (2008). Climate-induced variations of geyser periodicity in Yellowstone National Park, USA. *Geology*, *36*(6), 451–454. https://doi.org/10.1130/G24723A.1

Hurwitz, S., & Manga, M. (2017). The Fascinating and Complex Dynamics of Geyser Eruptions. *Annual Review of Earth and Planetary Sciences*, *45*, 31–59. https://doi.org/10.1146/annurev-earth-063016-015605

Husen, S., Taylor, R., Smith, R. B., & Healser, H. (2004). Changes in geyser eruption behavior and remotely triggered seismicity in Yellowstone National Park produced by the 2002 M 7.9 Denali fault earthquake, Alaska. *Geology*, *32*(6), 537–540. https://doi.org/10.1130/G20381.1

Iwase, T & Sakuma, Tetsuya & Yoshihisa, Koichi. (1997). Measurements on Sound Propagation Characteristics in Snow Layer. J Snow Eng of Jpn. 13.

Johnson, J. B. (1982). On the application of Biot's theory to acoustic wave propagation in snow. *Cold Regions Science and Technology*, *6*(1), 49-60.

Johnson, J. B., & Ripepe, M. (2011). Volcano infrasound: A review. *Journal of Volcanology and Geothermal Research*, *206*(3–4), 61–69. https://doi.org/10.1016/j.jvolgeores.2011.06.006

Johnson, J. B., Anderson, J. F., Anthony, R. E., & Sciotto, M. (2013). Detecting geyser activity with infrasound. *Journal of Volcanology and Geothermal Research*, *256*(April), 105–117. https://doi.org/10.1016/j.jvolgeores.2013.02.016

Karlstrom, L., Hurwitz, S., Sohn, R., Vandemeulebrouck, J., Murphy, F., Rudolph, M. L., Johnston, M. J. S., Manga, M., & McCleskey, R. B. (2013). Eruptions at Lone Star Geyser, Yellowstone National Park, USA: 1. Energetics and eruption dynamics. *Journal of Geophysical Research: Solid Earth*, *118*(8), 4048–4062. https://doi.org/10.1002/jgrb.50251

Kedar, S., Sturtevant, B., & Kanamori, H. (1996). The origin of harmonic tremor at Old Faithful geyser. *Nature*, *379*(6567), 708–711. https://doi.org/10.1038/379708a0

Keskinen, Z. (2023, in prep). Snow Attenuation of Infrasound Signals and Wind Noise.

Kieffer, S. W. (1989). Geologic nozzles. *Reviews of Geophysics*, *27*(1), 3–38. https://doi.org/10.1029/RG027i001p00003

Marcillo, O., Johnson, J. B., & Hart, D. (2012). Implementation, Characterization, and Evaluation of an Inexpensive Low-Power Low-Noise Infrasound Sensor Based on a Micromachined Differential Pressure Transducer and a Mechanical Filter. Journal of Atmospheric and Oceanic Technology, 29(9), 1275–1284. https://doi.org/10.1175/JTECH-D-11-00101.1

McKee, K., Fee, D., Yokoo, A., Matoza, R. S., & Kim, K. (2017). Analysis of gas jetting and fumarole acoustics at Aso Volcano, Japan. *Journal of Volcanology and Geothermal Research*, *340*, 16–29. https://doi.org/10.1016/j.jvolgeores.2017.03.029

Morgan, L. A., Shanks, W. C. P., Pierce, K. L., & Geological Society of America. (2009). *Hydrothermal processes above the yellowstone magma chamber : large hydrothermal systems and large hydrothermal explosions* (Ser. Special paper, 459). Geological Society of America.

Muffler, L. J. P., White, D. E., & Truesdell, A. H. (1971). Hydrothermal explosion craters in Yellowstone National Park. *Bulletin of the Geological Society of America*, *82*(3), 723–740. https://doi.org/10.1130/0016-7606(1971)82[723:HECIYN]2.0.CO;2

Mutschlecner, J. P., & Whitaker, R. W. (2005). Infrasound from earthquakes. *Journal of Geophysical Research D: Atmospheres*, *110*(1), 1–11. https://doi.org/10.1029/2004JD005067

Nayak, A., Manga, M., Hurwitz, S.,Namiki, A., & Dawson, P. B. (2020). Origin and properties of hydrothermal tremor at Lone Star Geyser,Yellowstone National Park, USA.Journal of Geophysical Research: SolidEarth,125, e2020JB019711. https://doi.org/10.1029/2020JB019711

Reed, M. H., Munoz-Saez, C., Hajimirza, S., Wu, S. M., Barth, A., Girona, T., Rasht-Behesht, M., White, E. B., Karplus, M. S., Hurwitz, S., & Manga, M. (2021). The 2018 reawakening and eruption dynamics of Steamboat Geyser, the world's tallest active geyser. *Proceedings of the National Academy of Sciences of the United States of America*, *118*(2). https://doi.org/10.1073/pnas.2020943118

Rinehart, J. S. (1974), Geysers, Eos Trans. AGU, 55( 12), 1052– 1062, doi:10.1029/EO055i012p01052.

Slad, G., & Merchant, B. (2021). Evaluation of Low Cost Infrasound Sensor Packages. (Issue September). https://doi.org/10.2172/1829264

USGS. (2015). *Hydrothermal Explosions*. USGS Yellowstone Hazards. https://volcanoes.usgs.gov/volcanoes/yellowstone/hazard_hydrothermal_explosion.html

USGS. (2022). Yellowstone Volcano Observatory Valve: Norris Temperatures, Steamboat, 2021. Data set. Available on-line [https://yvo-valve.wr.usgs.gov/] from United States Geological Survey Volcano Science Center.

Vandemeulebrouck, J., Roux, P., & Cros, E. (2013). The plumbing of Old Faithful Geyser revealed by hydrothermal tremor. *Geophysical Research Letters*, *40*(10), 1989–1993. https://doi.org/10.1002/grl.50422

Watson, L. M., Carpenter, B., Thompson, K., & Johnson, J. B. (2022). Using local infrasound arrays to detect plunging snow avalanches along the Milford Road, New Zealand (Aotearoa). *Natural Hazards*, *111*(1), 949–972. https://doi.org/10.1007/s11069-021-05086-w

White, D. E.(1967). Some principles of geyser activity, mainly from Steamboat Springs, Nevada. *American Journal of Science, Vol.* 265, p. 641-684.

White, D. E., Hutchinson, R. A., & Keith, T. E. C. (1988). The geology and remarkable thermal activity of Norris Geyser Basin, Yellowstone National Park, Wyoming. *US Geological Survey Professional Paper*, *1456*. https://doi.org/10.3133/pp1456

Wu, S. M., Lin, F. C., Farrell, J., Keller, W. E., White, E. B., & Hungerford, J. D. G. (2021). Imaging the Subsurface Plumbing Complex of Steamboat Geyser and Cistern Spring With Hydrothermal Tremor Migration Using Seismic Interferometry. Journal of Geophysical Research: Solid Earth, 126(4). https://doi.org/10.1029/2020JB021128

# APPENDIX A

## Infrasound Waveforms and Spectra for Major Eruptions at Steamboat Geyser

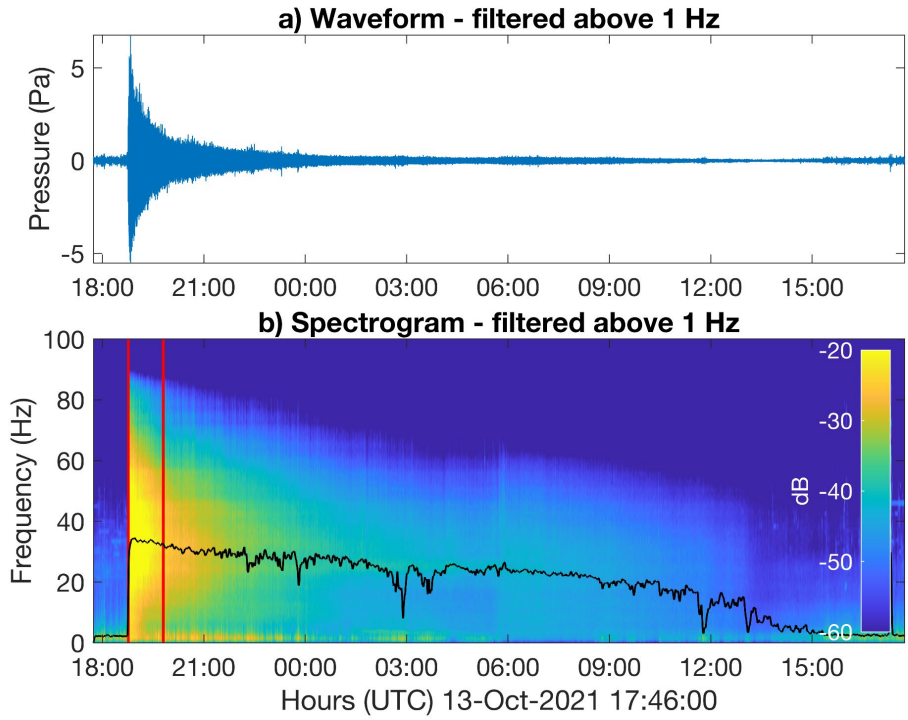
a) Waveform - filtered above 1 Hz
Pressure (Pa)
5
0
-5
18:00
21:00
00:00
03:00
06:00
09:00
12:00
15:00
b) Spectrogram - filtered above 1 Hz
Frequency (Hz)
100
80
60
40
20
0
dB
-20
-30
-40
-50
-60
Hours (UTC) 13-Oct-2021 17:46:00

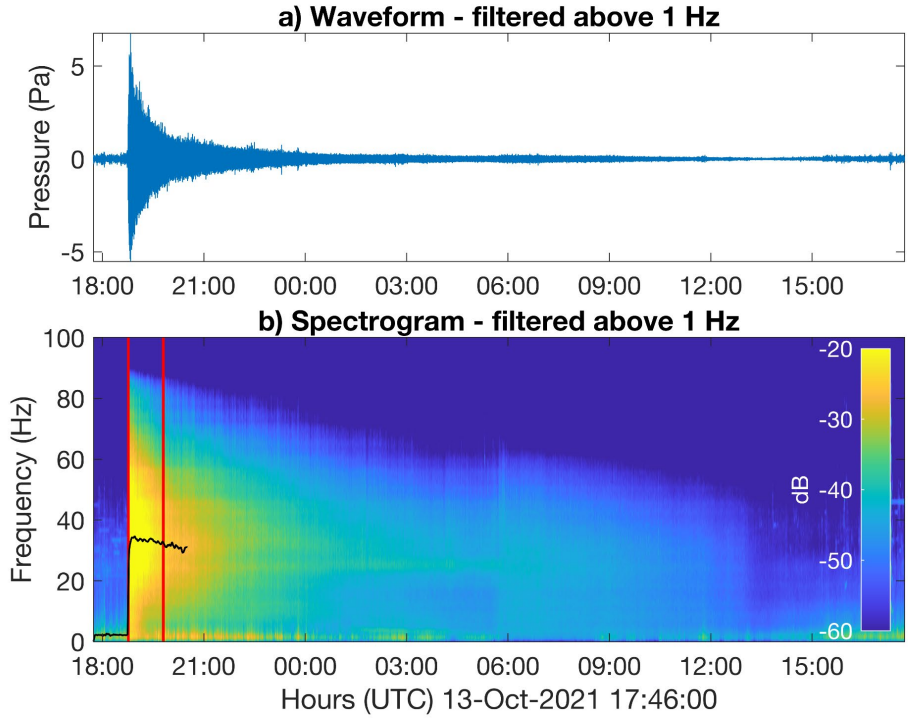
a) Waveform - filtered above 1 Hz
Pressure (Pa)
5
0
-5
18:00
21:00
00:00
03:00
06:00
09:00
12:00
15:00
b) Spectrogram - filtered above 1 Hz
Frequency (Hz)
100
80
60
40
20
0
dB
-20
-30
-40
-50
-60
Hours (UTC) 13-Oct-2021 17:46:00

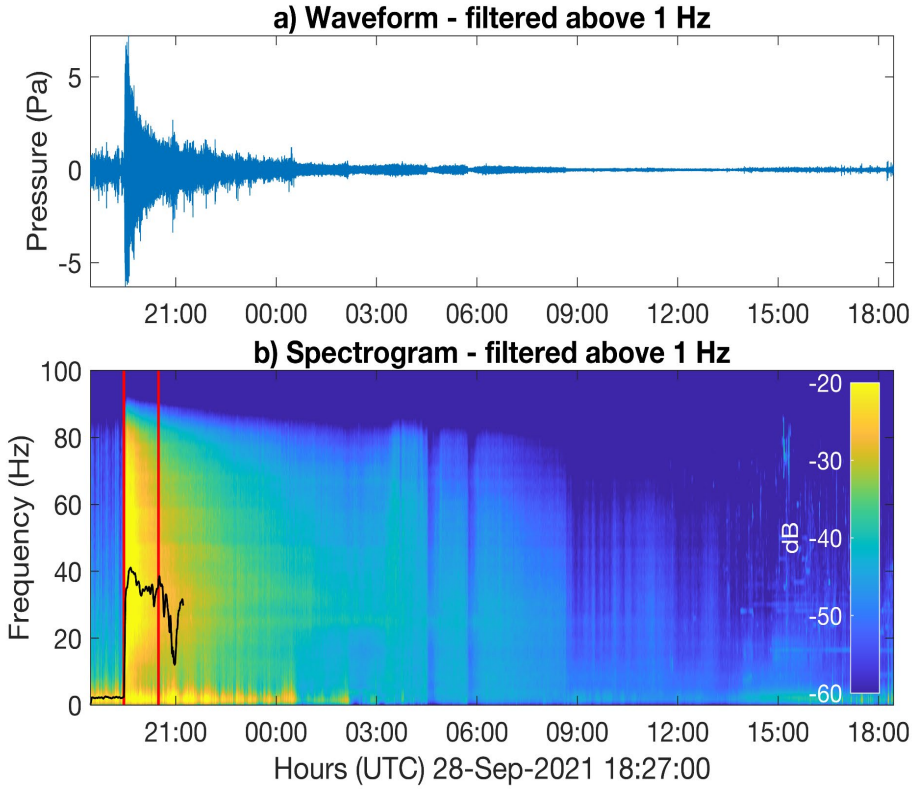
a) Waveform - filtered above 1 Hz
Pressure (Pa)
5
0
-5
21:00
00:00
03:00
06:00
09:00
12:00
15:00
18:00
b) Spectrogram - filtered above 1 Hz
Frequency (Hz)
100
80
60
40
20
0
dB
-20
-30
-40
-50
-60
Hours (UTC) 28-Sep-2021 18:27:00

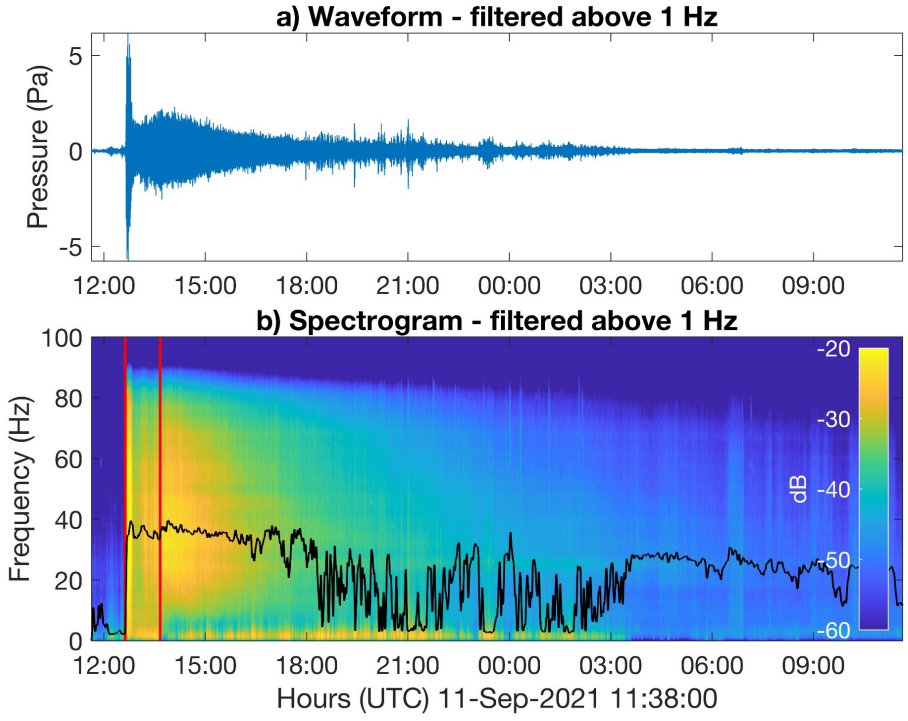
a) Waveform - filtered above 1 Hz
Pressure (Pa)
5
0
-5
12:00
15:00
18:00
21:00
00:00
03:00
06:00
09:00
b) Spectrogram - filtered above 1 Hz
Frequency (Hz)
100
80
60
40
20
0
dB
-20
-30
-40
-50
-60
Hours (UTC) 11-Sep-2021 11:38:00

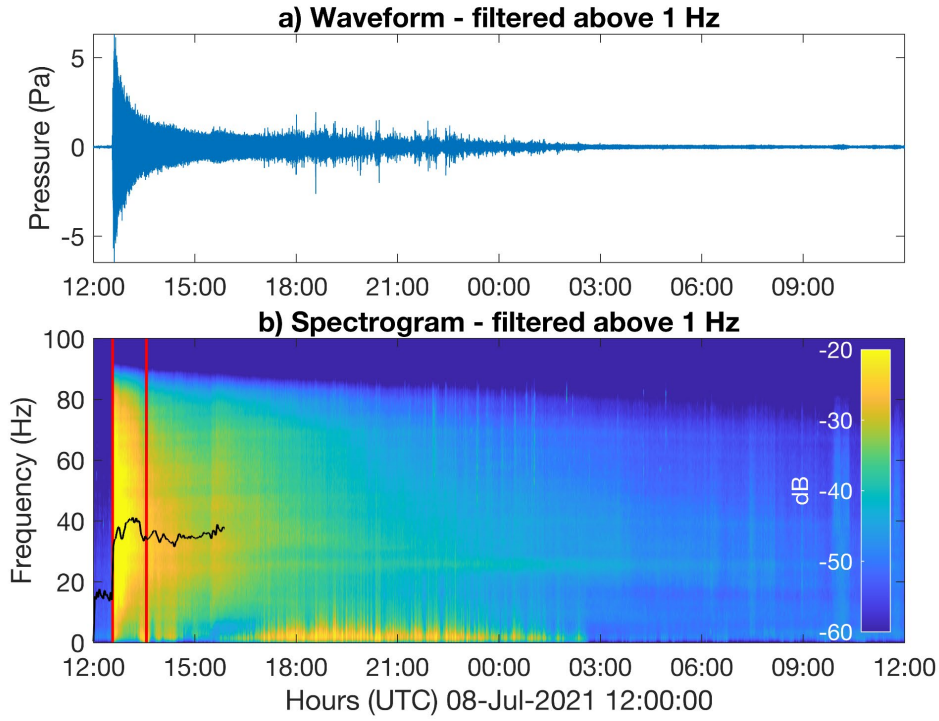
a) Waveform - filtered above 1 Hz
Pressure (Pa)
5
0
-5
12:00
15:00
18:00
21:00
00:00
03:00
06:00
09:00
b) Spectrogram - filtered above 1 Hz
Frequency (Hz)
100
80
60
40
20
0
dB
-20
-30
-40
-50
-60
12:00
15:00
18:00
21:00
00:00
03:00
06:00
09:00
12:00
Hours (UTC) 08-Jul-2021 12:00:00

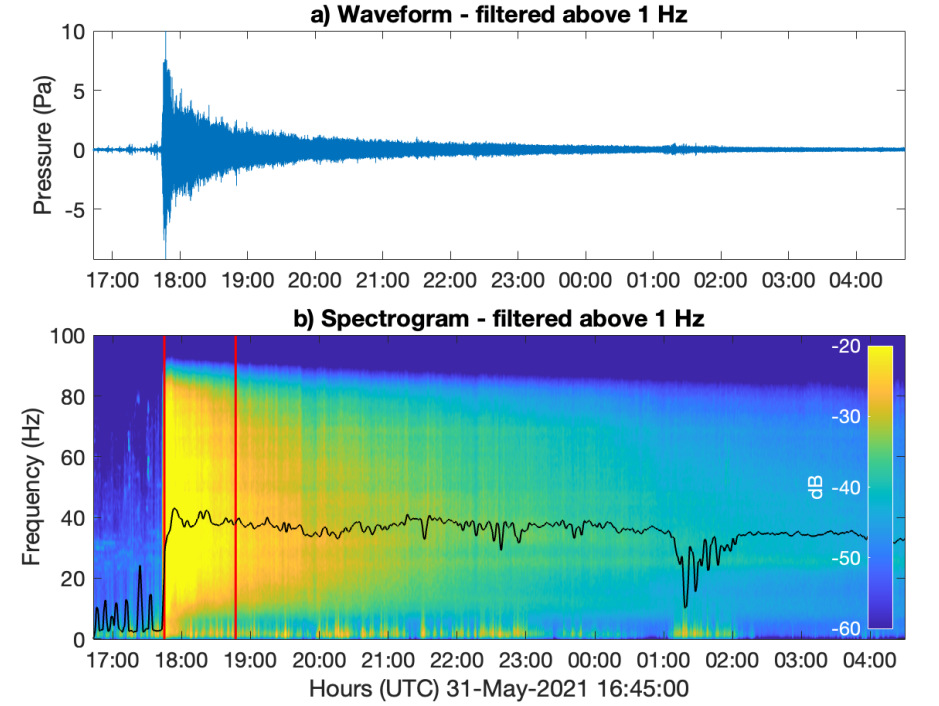
a) Waveform - filtered above 1 Hz
Pressure (Pa)
10
5
0
-5
17:00
18:00
19:00
20:00
21:00
22:00
23:00
00:00
01:00
02:00
03:00
04:00
b) Spectrogram - filtered above 1 Hz
Frequency (Hz)
100
80
60
40
20
0
dB
-20
-30
-40
-50
-60
17:00
18:00
19:00
20:00
21:00
22:00
23:00
00:00
01:00
02:00
03:00
04:00
Hours (UTC) 31-May-2021 16:45:00

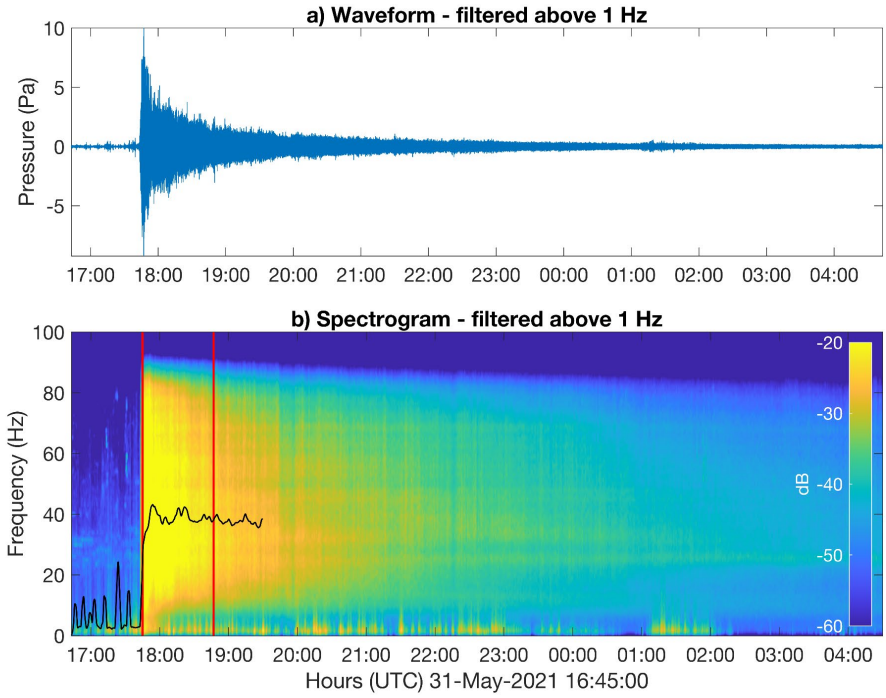
a) Waveform - filtered above 1 Hz
Pressure (Pa)
10
5
0
-5
17:00
18:00
19:00
20:00
21:00
22:00
23:00
00:00
01:00
02:00
03:00
04:00
b) Spectrogram - filtered above 1 Hz
Frequency (Hz)
100
80
60
40
20
0
dB
-20
-30
-40
-50
-60
Hours (UTC) 31-May-2021 16:45:00

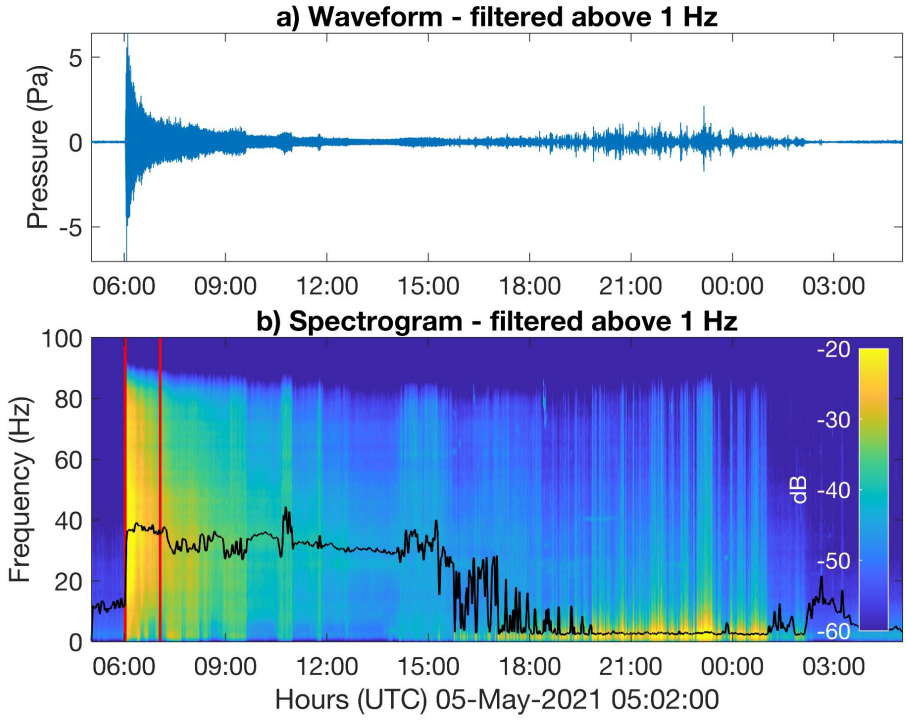
a) Waveform - filtered above 1 Hz
Pressure (Pa)
5
0
-5
06:00
09:00
12:00
15:00
18:00
21:00
00:00
03:00
b) Spectrogram - filtered above 1 Hz
Frequency (Hz)
100
80
60
40
20
0
dB
-20
-30
-40
-50
-60
Hours (UTC) 05-May-2021 05:02:00

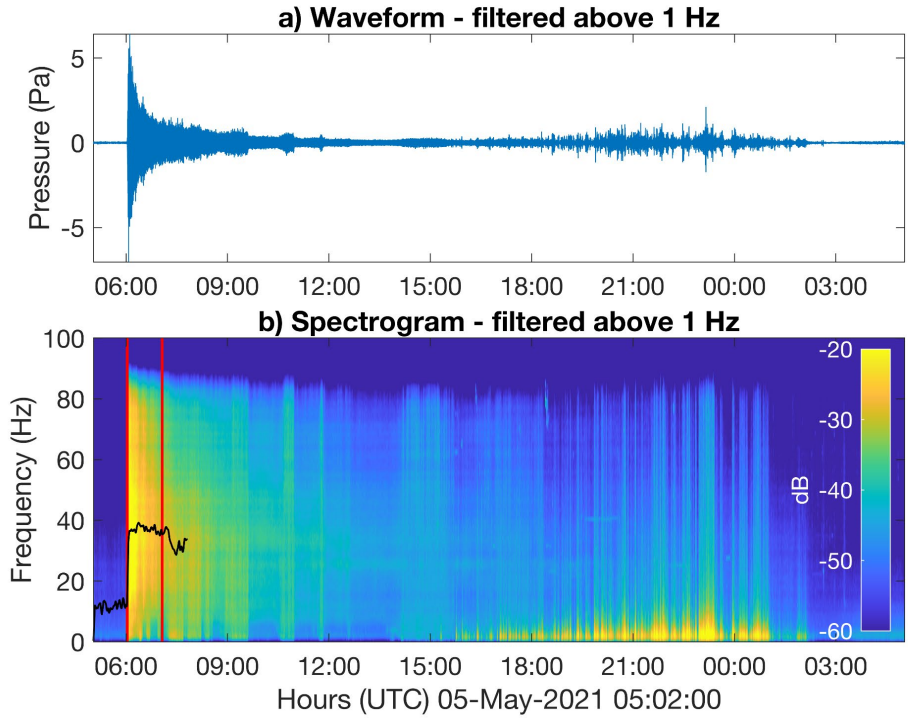
a) Waveform - filtered above 1 Hz
Pressure (Pa)
5
0
-5
06:00
09:00
12:00
15:00
18:00
21:00
00:00
03:00
b) Spectrogram - filtered above 1 Hz
Frequency (Hz)
100
80
60
40
20
0
dB
-20
-30
-40
-50
-60
Hours (UTC) 05-May-2021 05:02:00

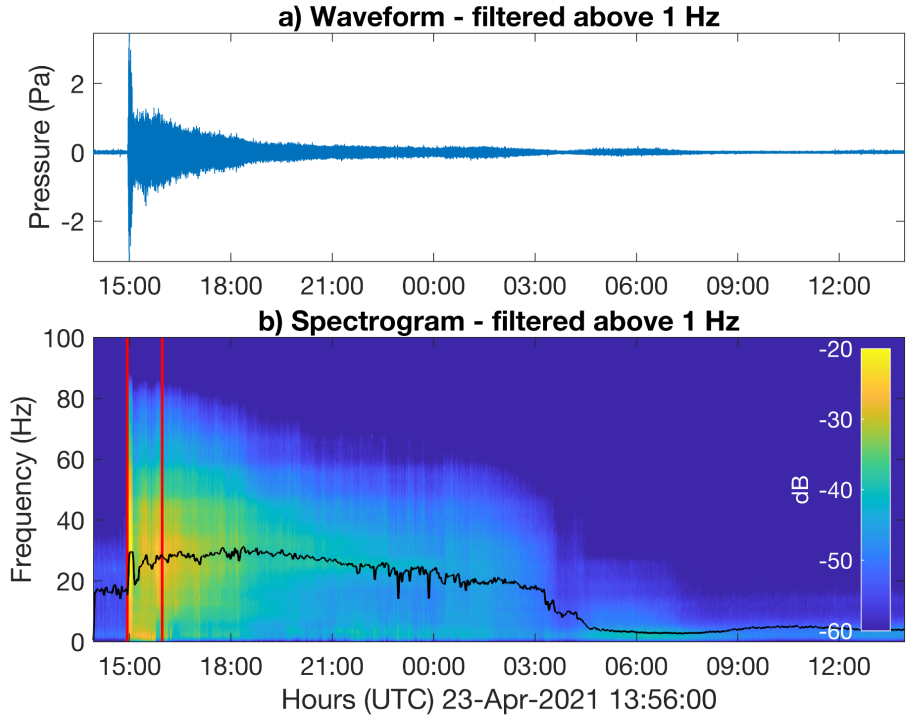
a) Waveform - filtered above 1 Hz
Pressure (Pa)
2
0
-2
15:00
18:00
21:00
00:00
03:00
06:00
09:00
12:00
b) Spectrogram - filtered above 1 Hz
Frequency (Hz)
100
80
60
40
20
0
dB
-20
-30
-40
-50
-60
Hours (UTC) 23-Apr-2021 13:56:00

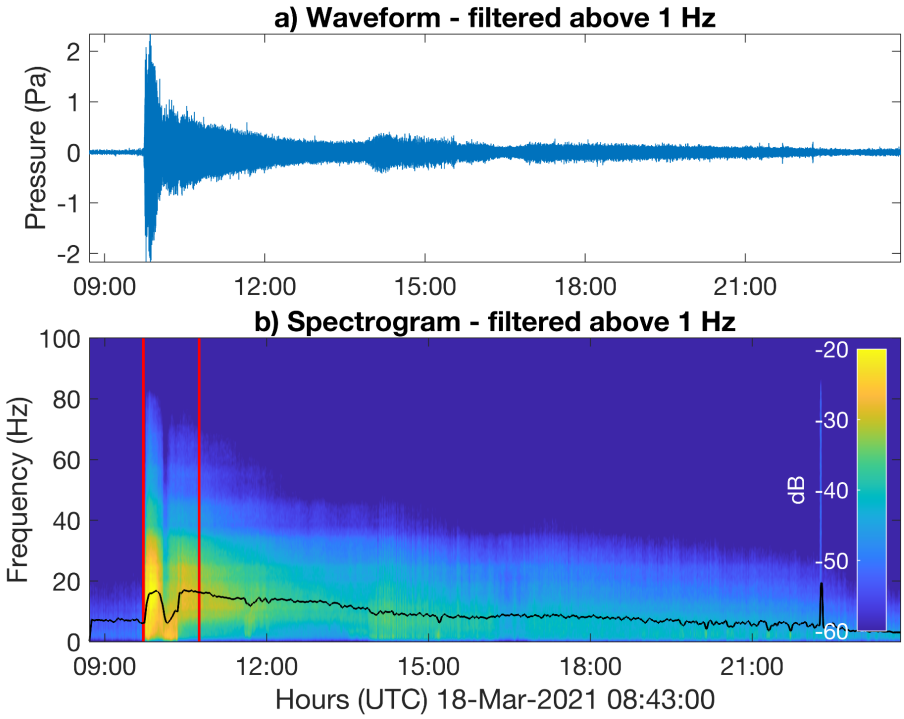


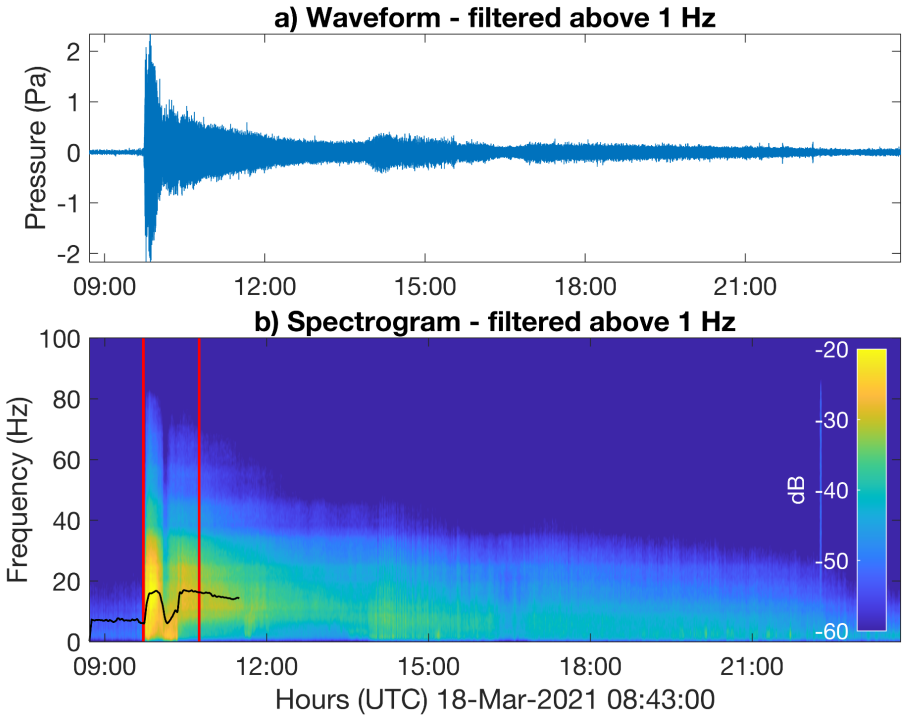


- Different length event

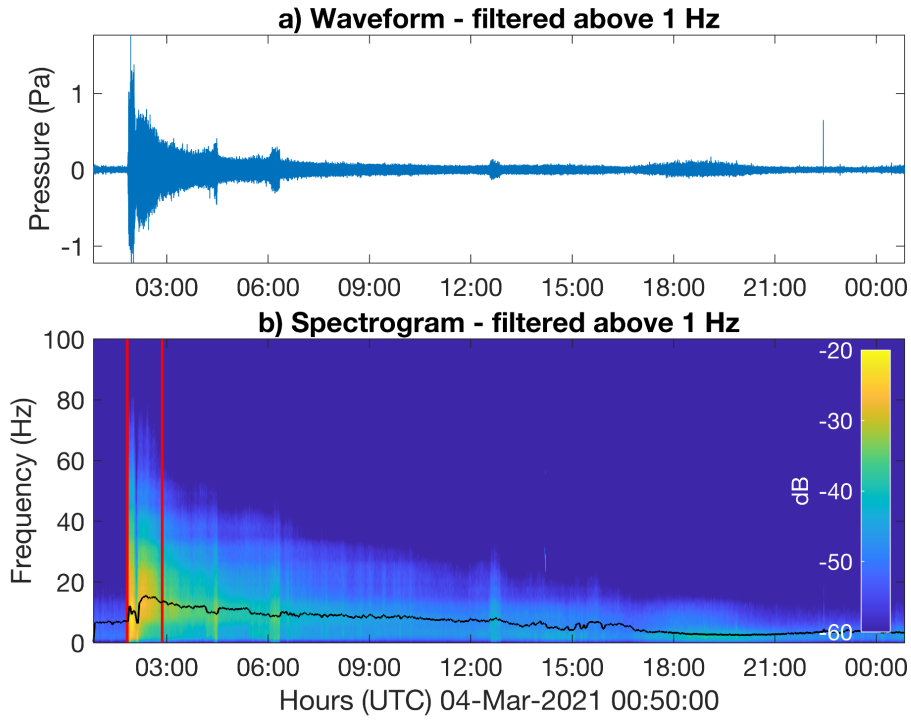
a) Waveform - filtered above 1 Hz
Pressure (Pa)
1
0
-1
03:00
06:00
09:00
12:00
15:00
18:00
21:00
00:00
b) Spectrogram - filtered above 1 Hz
Frequency (Hz)
100
80
60
40
20
0
dB
-20
-30
-40
-50
-60
03:00
06:00
09:00
12:00
15:00
18:00
21:00
00:00
Hours (UTC) 04-Mar-2021 00:50:00

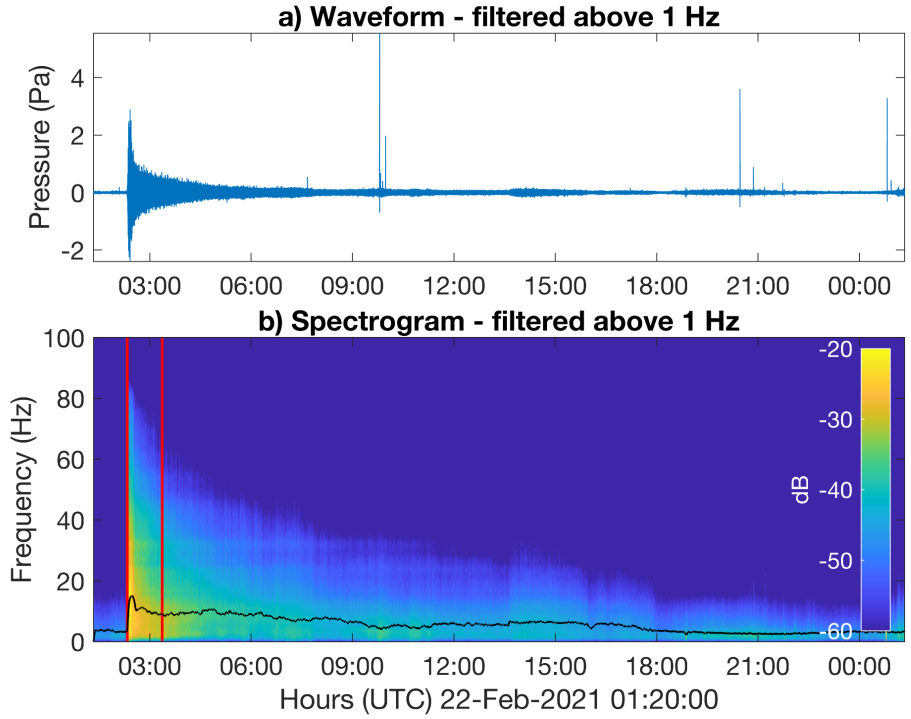
a) Waveform - filtered above 1 Hz
Pressure (Pa)
4
2
0
-2
03:00
06:00
09:00
12:00
15:00
18:00
21:00
00:00
b) Spectrogram - filtered above 1 Hz
Frequency (Hz)
100
80
60
40
20
0
dB
-20
-30
-40
-50
-60
03:00
06:00
09:00
12:00
15:00
18:00
21:00
00:00
Hours (UTC) 22-Feb-2021 01:20:00

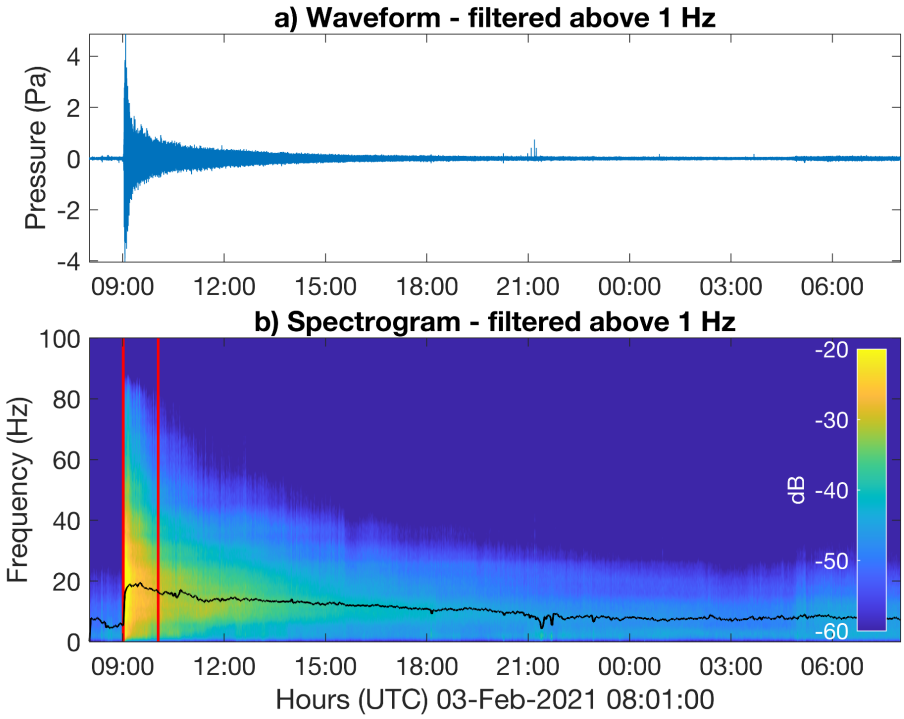
a) Waveform - filtered above 1 Hz
Pressure (Pa)
4
2
0
-2
-4
09:00
12:00
15:00
18:00
21:00
00:00
03:00
06:00
b) Spectrogram - filtered above 1 Hz
Frequency (Hz)
100
80
60
40
20
0
dB
-20
-30
-40
-50
-60
09:00
12:00
15:00
18:00
21:00
00:00
03:00
06:00
Hours (UTC) 03-Feb-2021 08:01:00

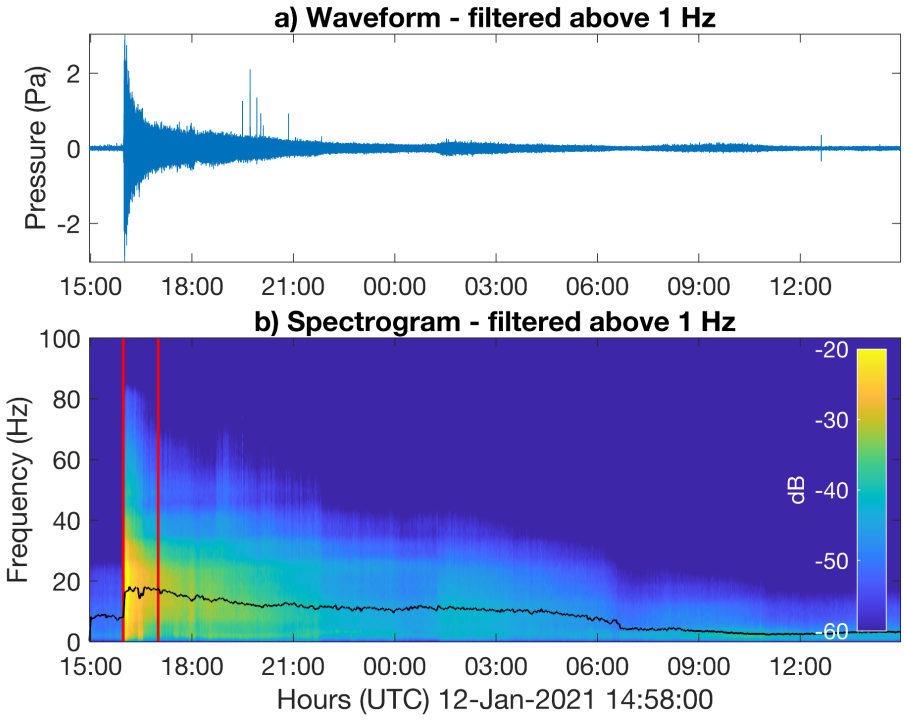
a) Waveform - filtered above 1 Hz
Pressure (Pa)
2
0
-2
15:00
18:00
21:00
00:00
03:00
06:00
09:00
12:00
b) Spectrogram - filtered above 1 Hz
Frequency (Hz)
100
80
60
40
20
0
dB
-20
-30
-40
-50
-60
15:00
18:00
21:00
00:00
03:00
06:00
09:00
12:00
Hours (UTC) 12-Jan-2021 14:58:00

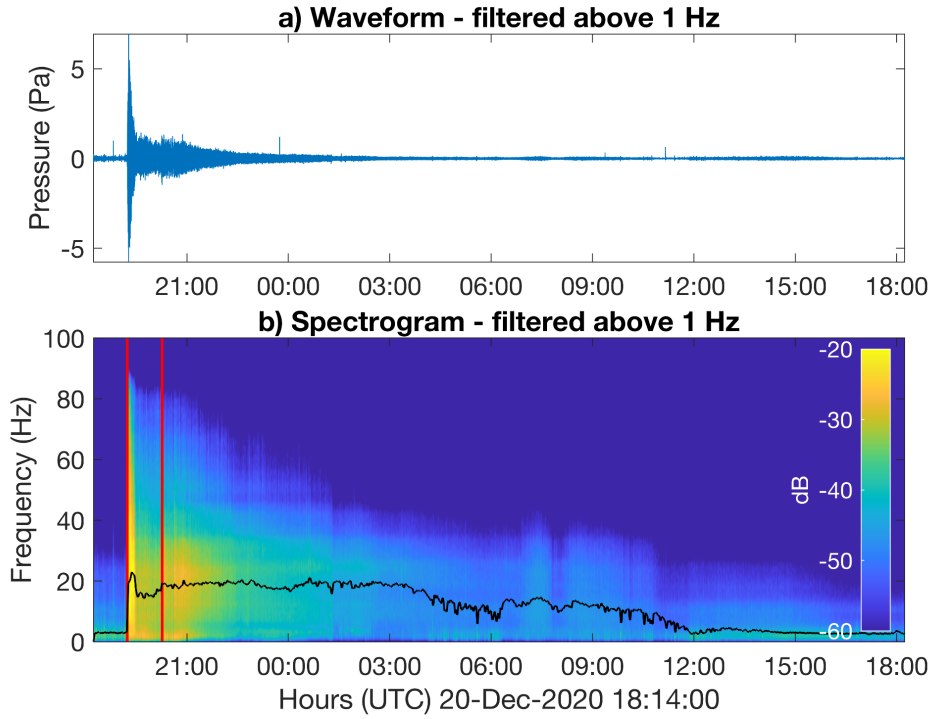
a) Waveform - filtered above 1 Hz
Pressure (Pa)
5
0
-5
21:00
00:00
03:00
06:00
09:00
12:00
15:00
18:00
b) Spectrogram - filtered above 1 Hz
Frequency (Hz)
100
80
60
40
20
0
dB
-20
-30
-40
-50
-60
Hours (UTC) 20-Dec-2020 18:14:00

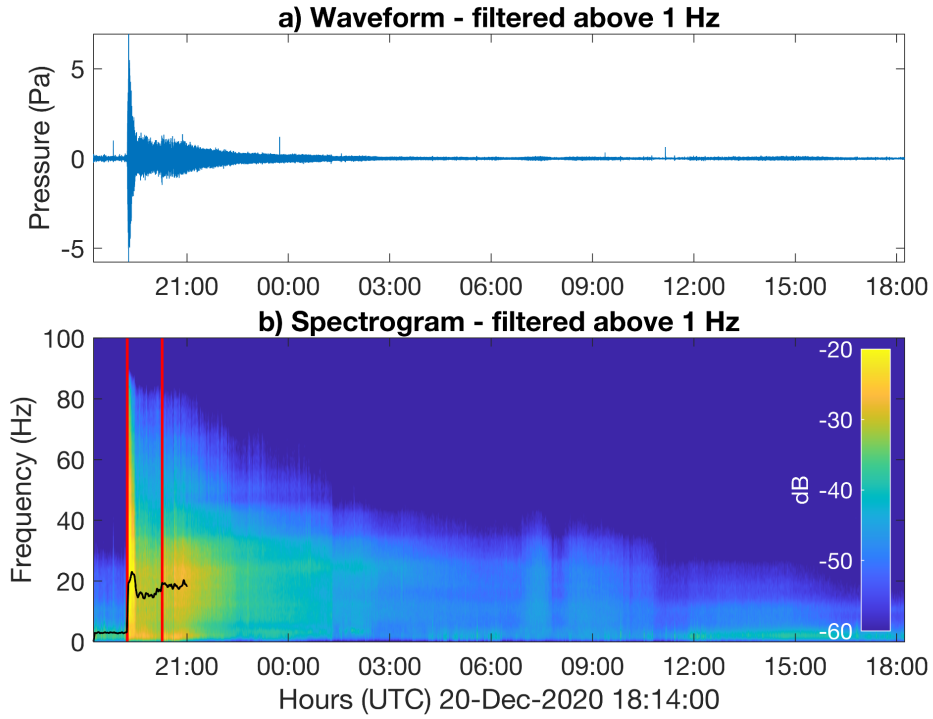
a) Waveform - filtered above 1 Hz
Pressure (Pa)
5
0
-5
21:00
00:00
03:00
06:00
09:00
12:00
15:00
18:00
b) Spectrogram - filtered above 1 Hz
Frequency (Hz)
100
80
60
40
20
0
dB
-20
-30
-40
-50
-60
Hours (UTC) 20-Dec-2020 18:14:00

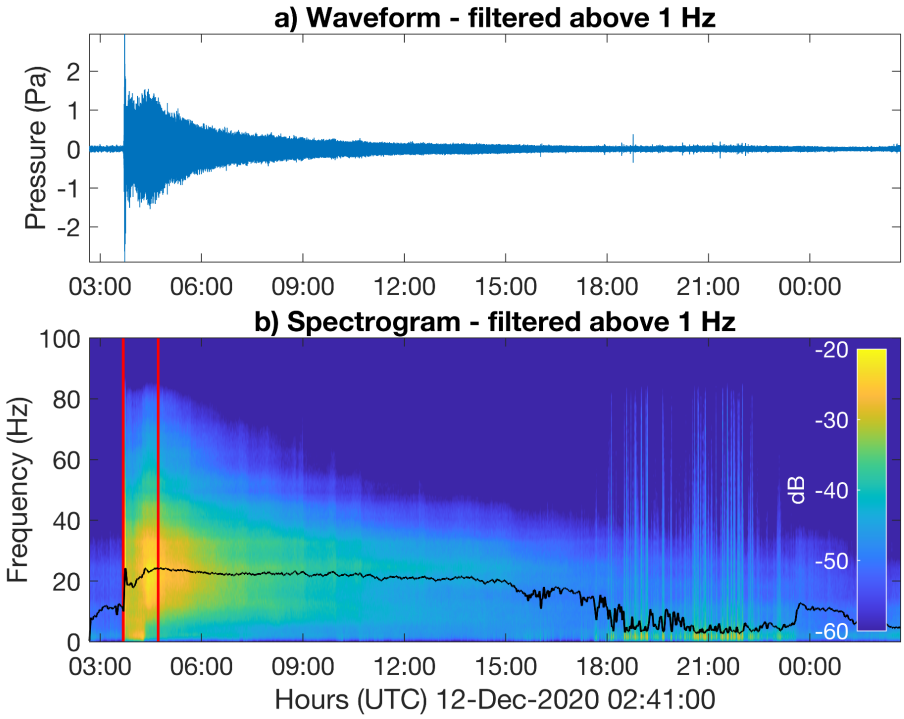
a) Waveform - filtered above 1 Hz
Pressure (Pa)
2
1
0
-1
-2
03:00
06:00
09:00
12:00
15:00
18:00
21:00
00:00
b) Spectrogram - filtered above 1 Hz
Frequency (Hz)
100
80
60
40
20
0
dB
-20
-30
-40
-50
-60
Hours (UTC) 12-Dec-2020 02:41:00

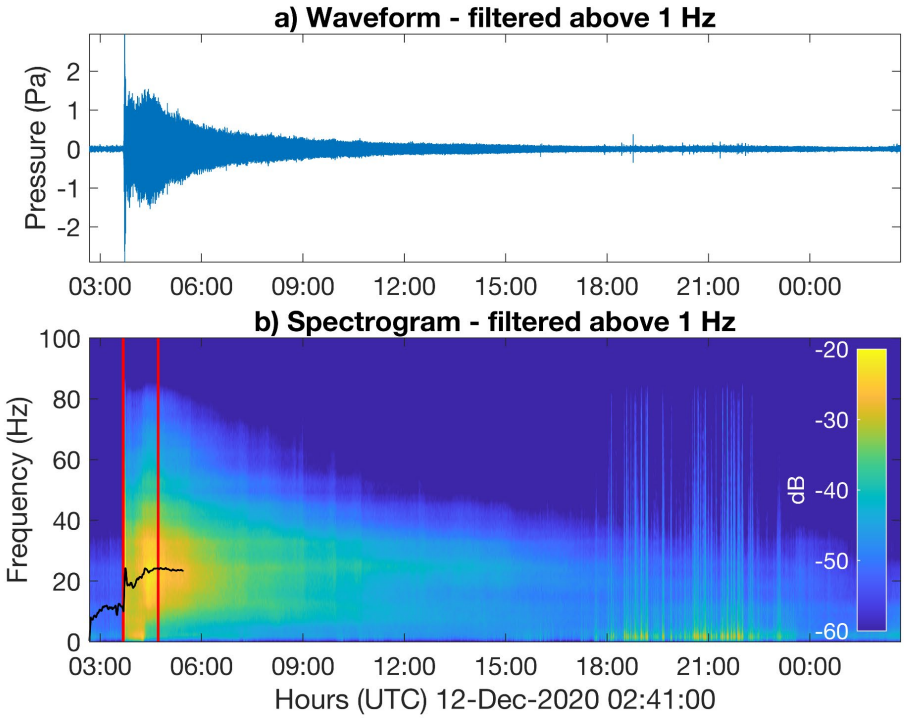
a) Waveform - filtered above 1 Hz
Pressure (Pa)
2
1
0
-1
-2
03:00
06:00
09:00
12:00
15:00
18:00
21:00
00:00
b) Spectrogram - filtered above 1 Hz
Frequency (Hz)
100
80
60
40
20
0
dB
-20
-30
-40
-50
-60
Hours (UTC) 12-Dec-2020 02:41:00

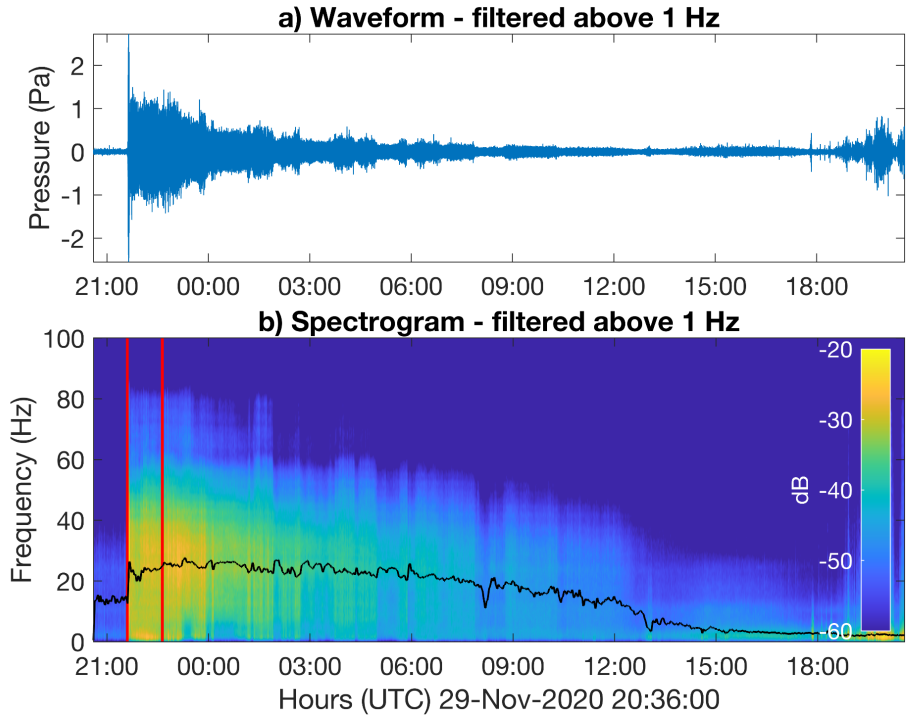
a) Waveform - filtered above 1 Hz
Pressure (Pa)
2
1
0
-1
-2
21:00
00:00
03:00
06:00
09:00
12:00
15:00
18:00
b) Spectrogram - filtered above 1 Hz
Frequency (Hz)
100
80
60
40
20
0
dB
-20
-30
-40
-50
-60
Hours (UTC) 29-Nov-2020 20:36:00

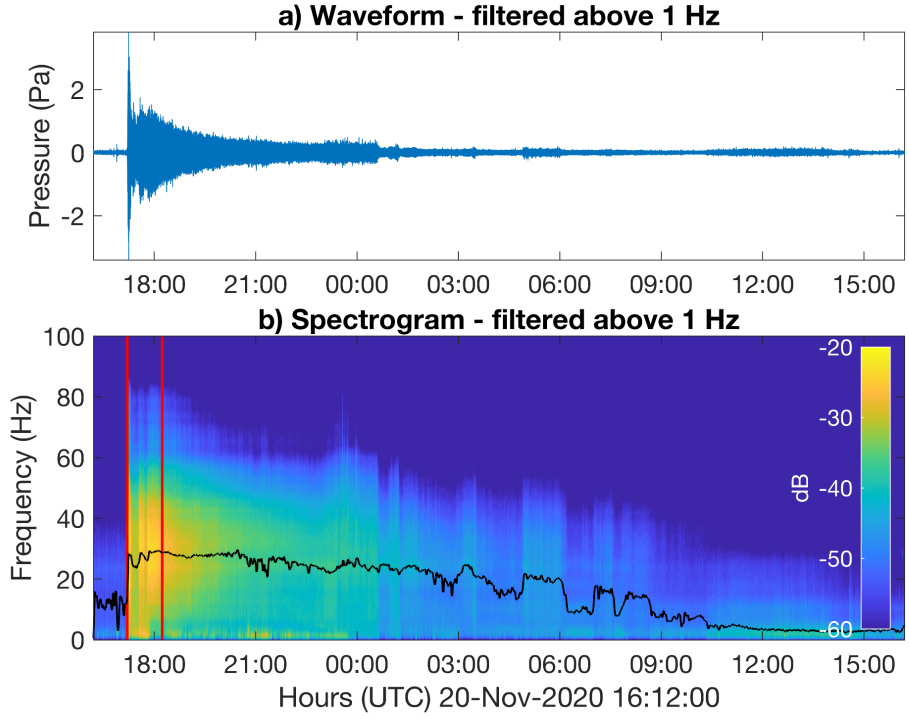
a) Waveform - filtered above 1 Hz
Pressure (Pa)
2
0
-2
18:00
21:00
00:00
03:00
06:00
09:00
12:00
15:00
b) Spectrogram - filtered above 1 Hz
Frequency (Hz)
100
80
60
40
20
0
dB
-20
-30
-40
-50
-60
Hours (UTC) 20-Nov-2020 16:12:00

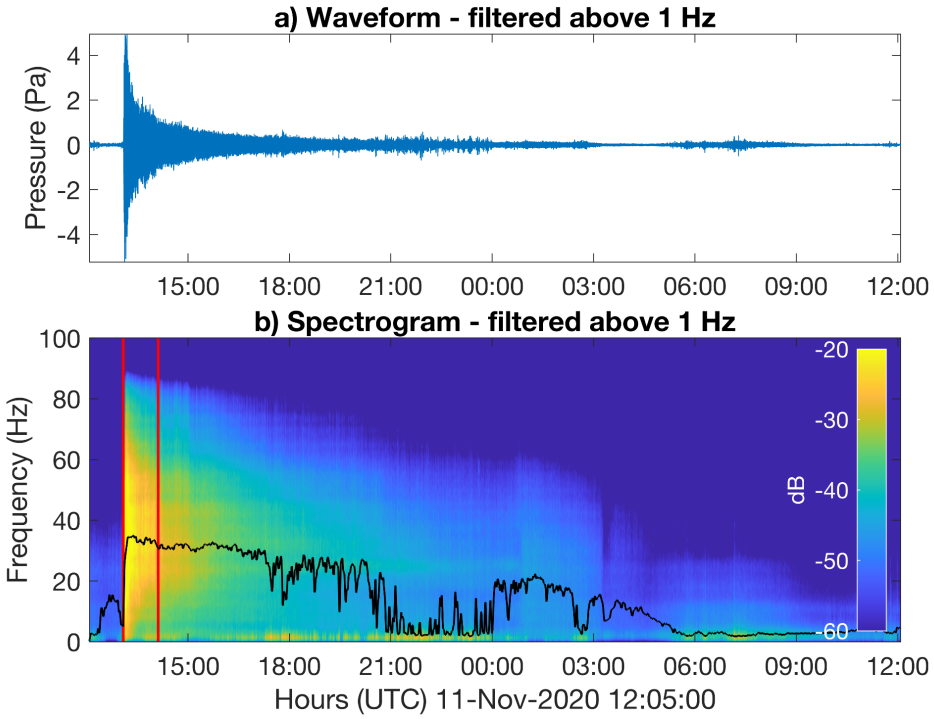
a) Waveform - filtered above 1 Hz
Pressure (Pa)
4
2
0
-2
-4
15:00
18:00
21:00
00:00
03:00
06:00
09:00
12:00
b) Spectrogram - filtered above 1 Hz
Frequency (Hz)
100
80
60
40
20
0
dB
-20
-30
-40
-50
-60
15:00
18:00
21:00
00:00
03:00
06:00
09:00
12:00
Hours (UTC) 11-Nov-2020 12:05:00

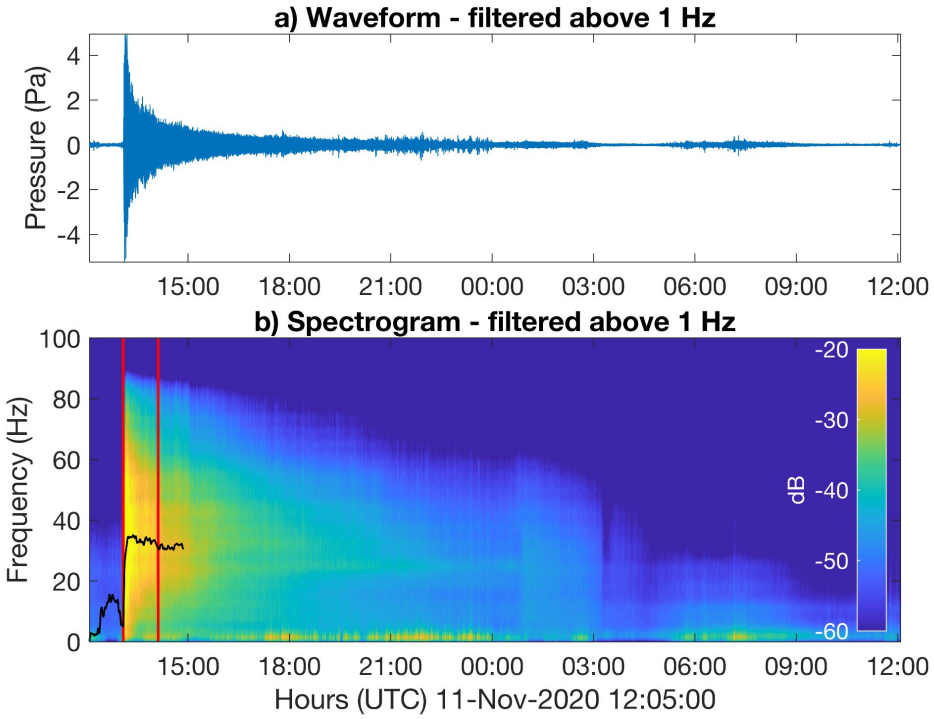
a) Waveform - filtered above 1 Hz
Pressure (Pa)
4
2
0
-2
-4
15:00
18:00
21:00
00:00
03:00
06:00
09:00
12:00
b) Spectrogram - filtered above 1 Hz
Frequency (Hz)
100
80
60
40
20
0
dB
-20
-30
-40
-50
-60
15:00
18:00
21:00
00:00
03:00
06:00
09:00
12:00
Hours (UTC) 11-Nov-2020 12:05:00

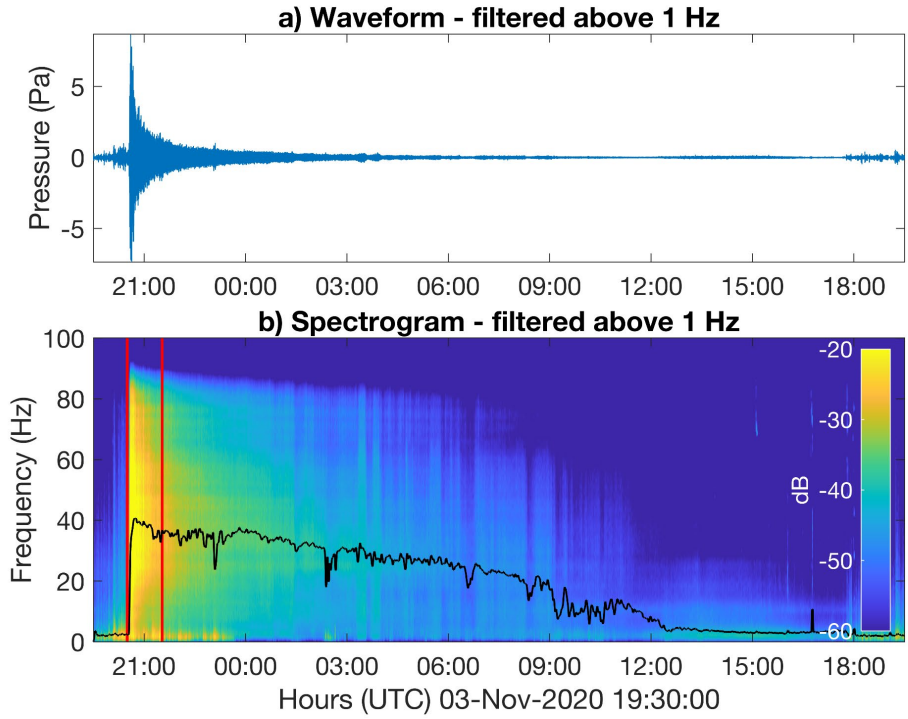
a) Waveform - filtered above 1 Hz
Pressure (Pa)
5
0
-5
21:00
00:00
03:00
06:00
09:00
12:00
15:00
18:00
b) Spectrogram - filtered above 1 Hz
Frequency (Hz)
100
80
60
40
20
0
dB
-20
-30
-40
-50
-60
21:00
00:00
03:00
06:00
09:00
12:00
15:00
18:00
Hours (UTC) 03-Nov-2020 19:30:00

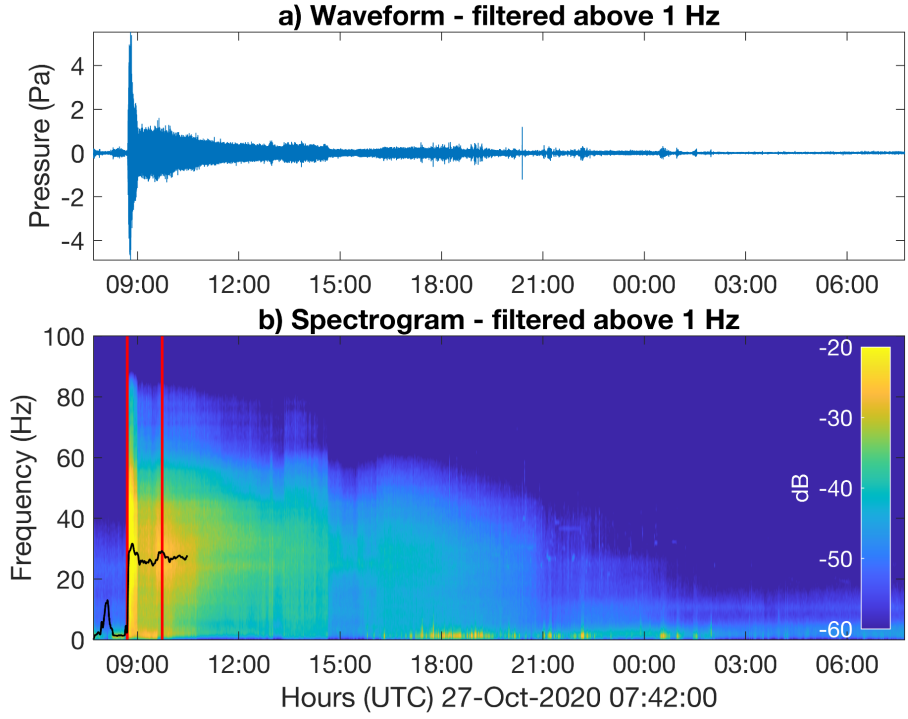
a) Waveform - filtered above 1 Hz
Pressure (Pa)
4
2
0
-2
-4
09:00
12:00
15:00
18:00
21:00
00:00
03:00
06:00
b) Spectrogram - filtered above 1 Hz
Frequency (Hz)
100
80
60
40
20
0
dB
-20
-30
-40
-50
-60
09:00
12:00
15:00
18:00
21:00
00:00
03:00
06:00
Hours (UTC) 27-Oct-2020 07:42:00

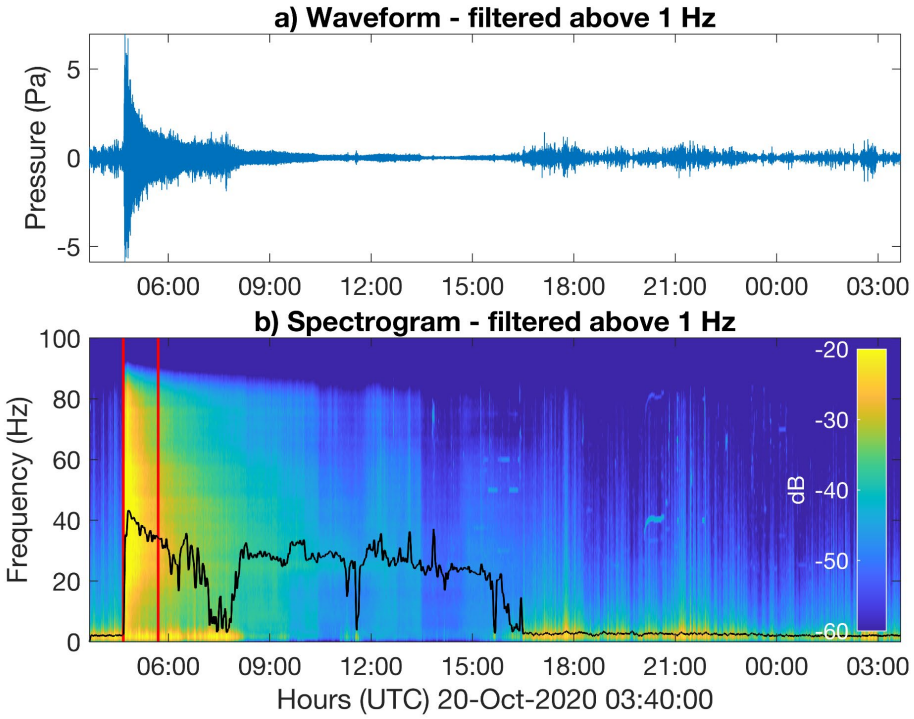
a) Waveform - filtered above 1 Hz
Pressure (Pa)
5
0
-5
06:00
09:00
12:00
15:00
18:00
21:00
00:00
03:00
b) Spectrogram - filtered above 1 Hz
Frequency (Hz)
100
80
60
40
20
0
dB
-20
-30
-40
-50
-60
Hours (UTC) 20-Oct-2020 03:40:00

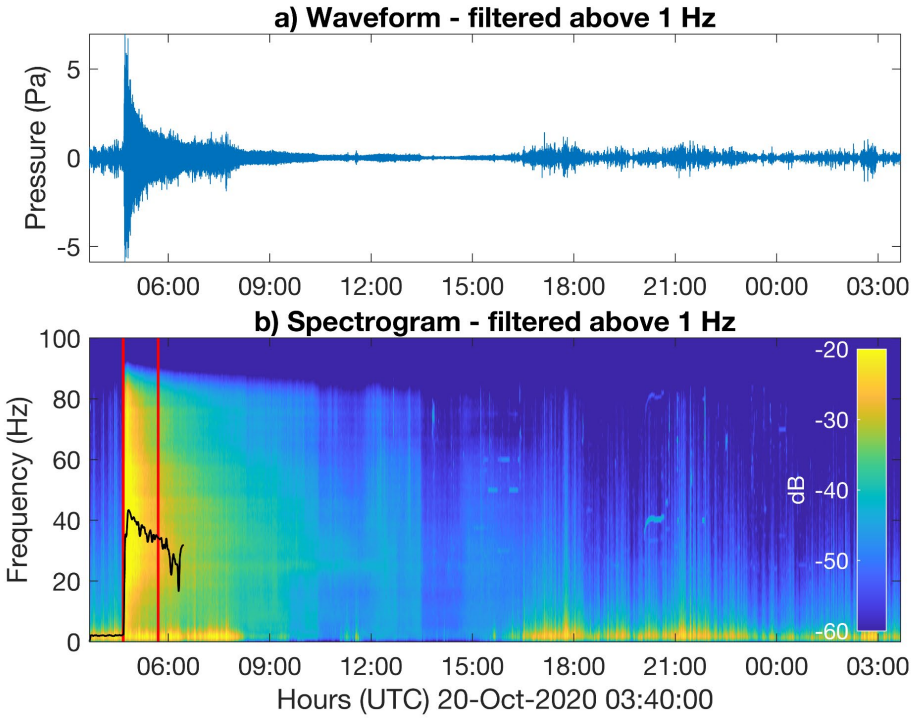
a) Waveform - filtered above 1 Hz
Pressure (Pa)
5
0
-5
06:00
09:00
12:00
15:00
18:00
21:00
00:00
03:00
b) Spectrogram - filtered above 1 Hz
Frequency (Hz)
100
80
60
40
20
0
dB
-20
-30
-40
-50
-60
Hours (UTC) 20-Oct-2020 03:40:00

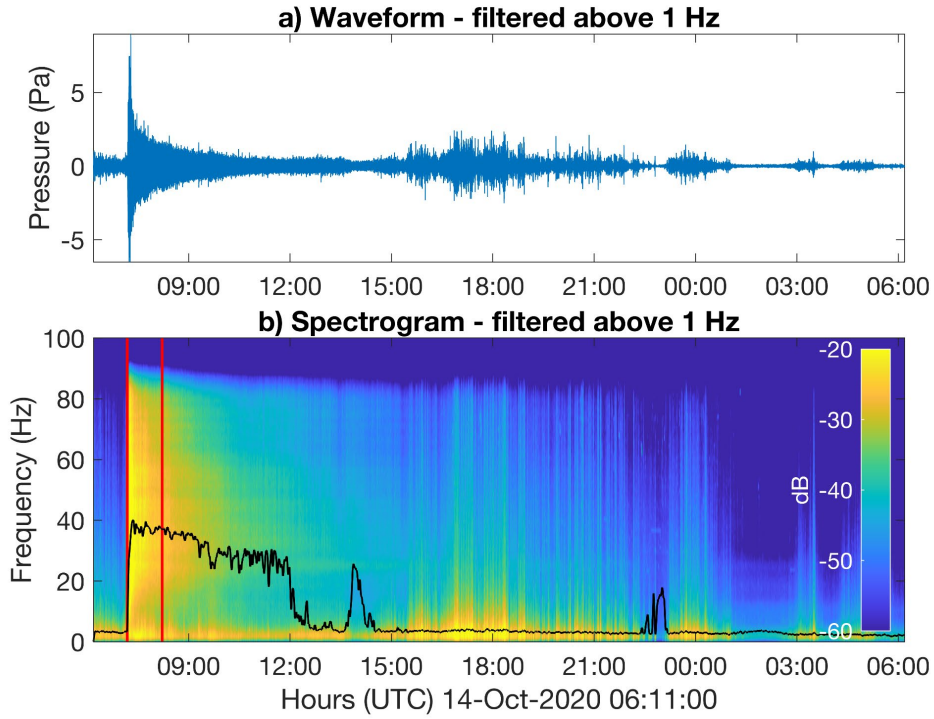
a) Waveform - filtered above 1 Hz
Pressure (Pa)
5
0
-5
09:00
12:00
15:00
18:00
21:00
00:00
03:00
06:00
b) Spectrogram - filtered above 1 Hz
Frequency (Hz)
100
80
60
40
20
0
dB
-20
-30
-40
-50
-60
09:00
12:00
15:00
18:00
21:00
00:00
03:00
06:00
Hours (UTC) 14-Oct-2020 06:11:00

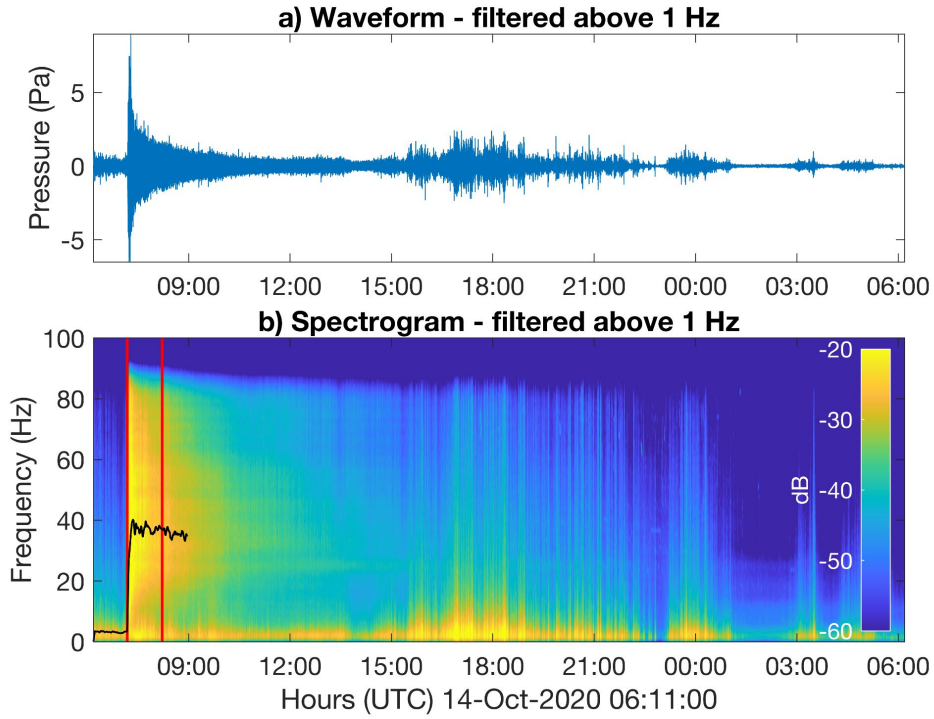
a) Waveform - filtered above 1 Hz
Pressure (Pa)
5
0
-5
09:00
12:00
15:00
18:00
21:00
00:00
03:00
06:00
b) Spectrogram - filtered above 1 Hz
Frequency (Hz)
100
80
60
40
20
0
dB
-20
-30
-40
-50
-60
09:00
12:00
15:00
18:00
21:00
00:00
03:00
06:00
Hours (UTC) 14-Oct-2020 06:11:00

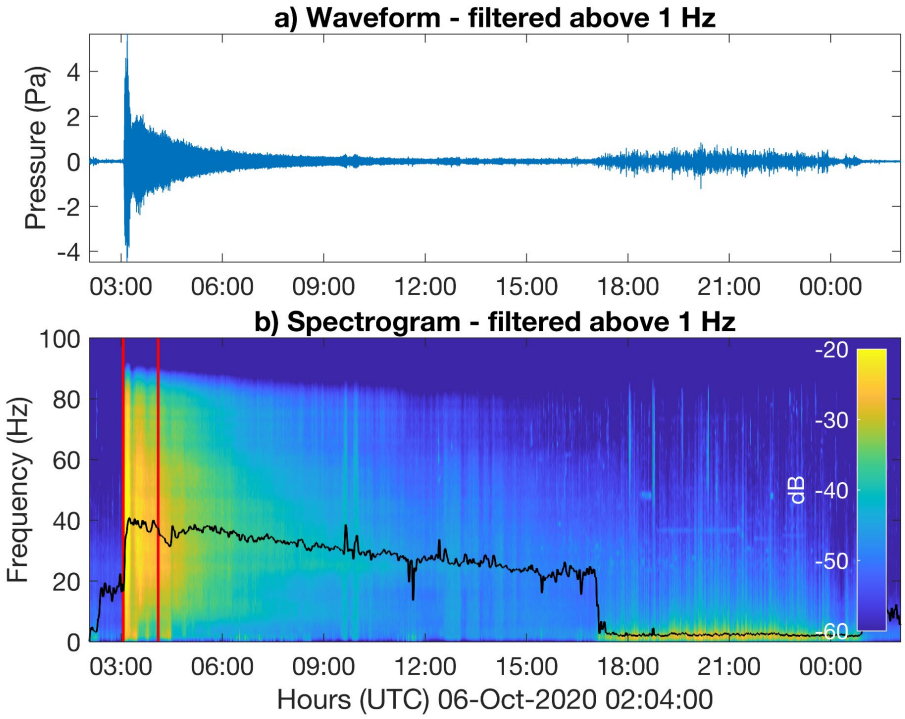
a) Waveform - filtered above 1 Hz
Pressure (Pa)
4
2
0
-2
-4
03:00
06:00
09:00
12:00
15:00
18:00
21:00
00:00
b) Spectrogram - filtered above 1 Hz
Frequency (Hz)
100
80
60
40
20
0
dB
-20
-30
-40
-50
-60
Hours (UTC) 06-Oct-2020 02:04:00

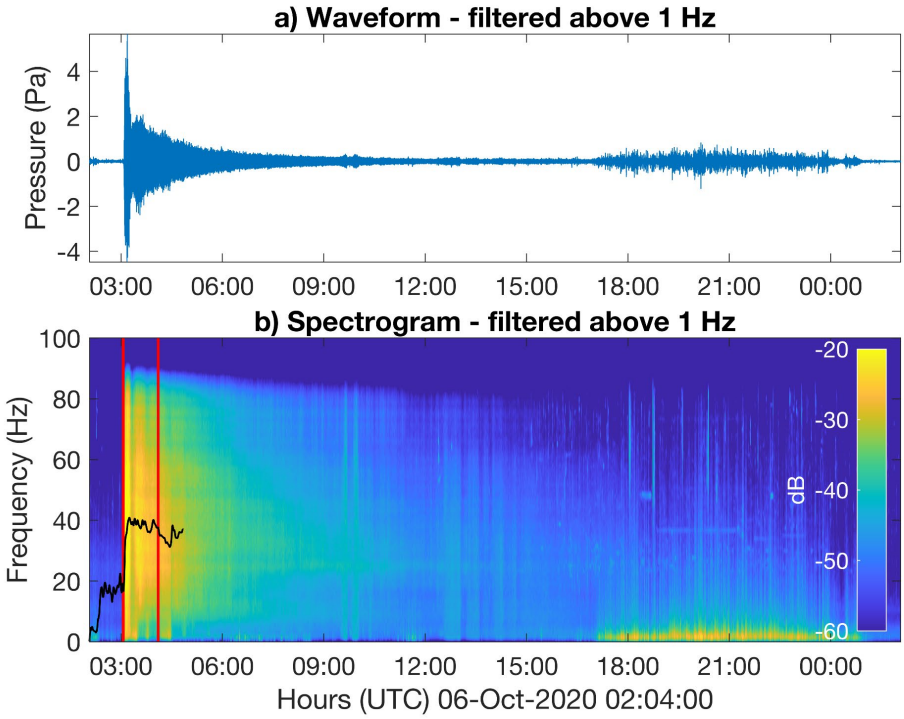
a) Waveform - filtered above 1 Hz
Pressure (Pa)
4
2
0
-2
-4
03:00
06:00
09:00
12:00
15:00
18:00
21:00
00:00
b) Spectrogram - filtered above 1 Hz
Frequency (Hz)
100
80
60
40
20
0
dB
-20
-30
-40
-50
-60
Hours (UTC) 06-Oct-2020 02:04:00

# APPENDIX B

## Infrasound Waveforms and Spectra for Non-eruption Days at Steamboat Geyser

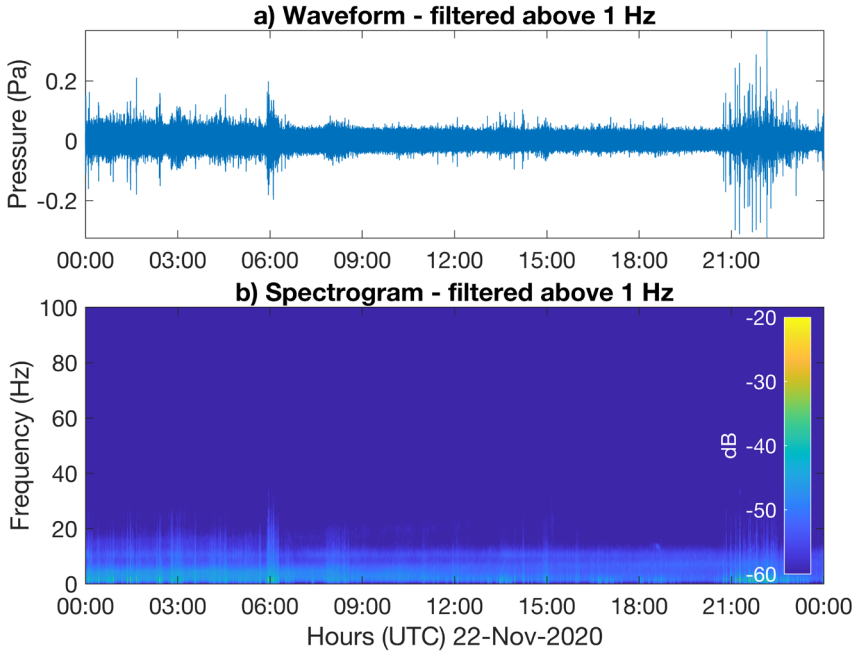
a) Waveform - filtered above 1 Hz
Pressure (Pa)
0.2
0
-0.2
00:00
03:00
06:00
09:00
12:00
15:00
18:00
21:00
b) Spectrogram - filtered above 1 Hz
Frequency (Hz)
100
80
60
40
20
0
dB
-20
-30
-40
-50
-60
00:00
Hours (UTC) 22-Nov-2020

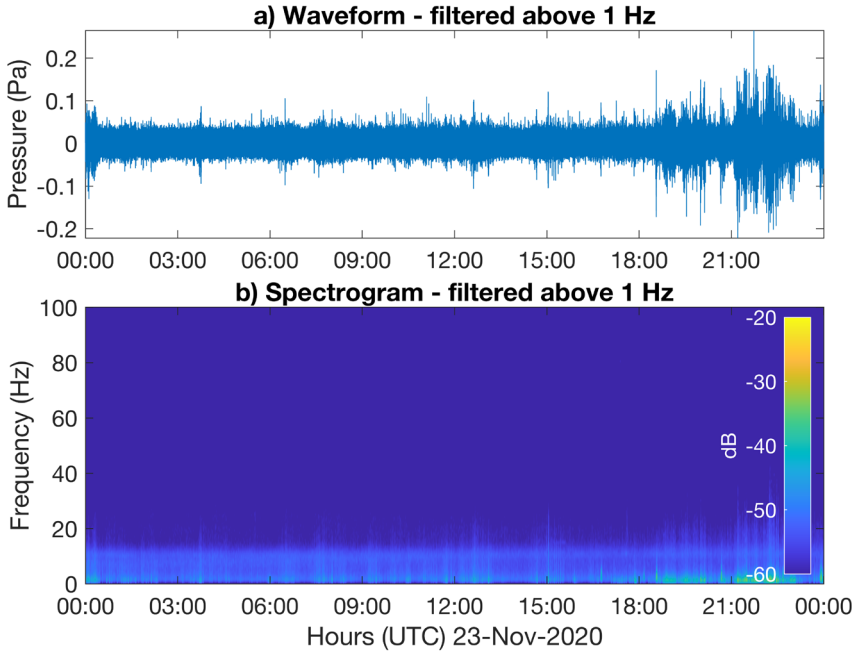
a) Waveform - filtered above 1 Hz
Pressure (Pa)
0.2
0.1
0
-0.1
-0.2
00:00
03:00
06:00
09:00
12:00
15:00
18:00
21:00
b) Spectrogram - filtered above 1 Hz
Frequency (Hz)
100
80
60
40
20
0
dB
-20
-30
-40
-50
-60
00:00
Hours (UTC) 23-Nov-2020

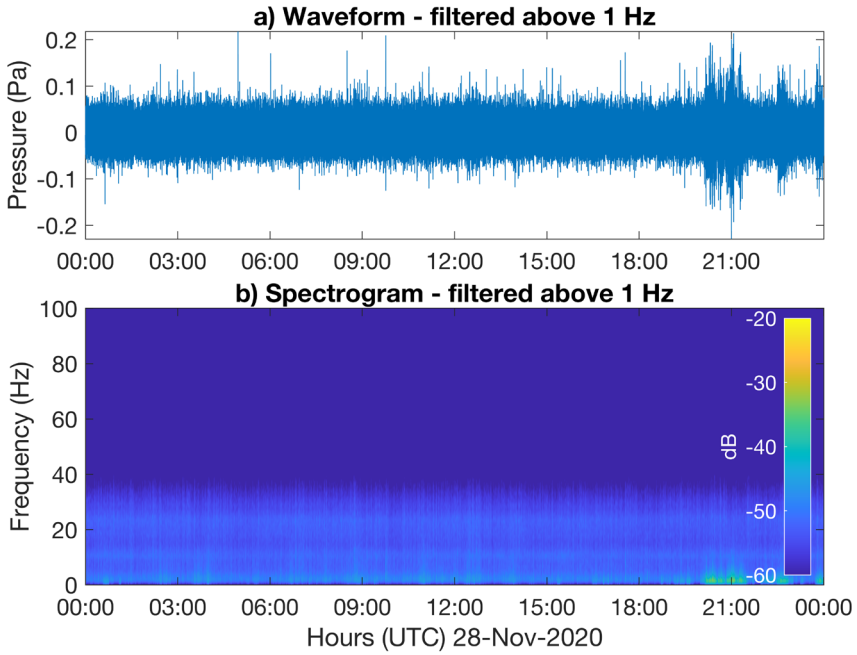
a) Waveform - filtered above 1 Hz
Pressure (Pa)
0.2
0.1
0
-0.1
-0.2
00:00
03:00
06:00
09:00
12:00
15:00
18:00
21:00
b) Spectrogram - filtered above 1 Hz
Frequency (Hz)
100
80
60
40
20
0
dB
-20
-30
-40
-50
-60
00:00
03:00
06:00
09:00
12:00
15:00
18:00
21:00
00:00
Hours (UTC) 28-Nov-2020

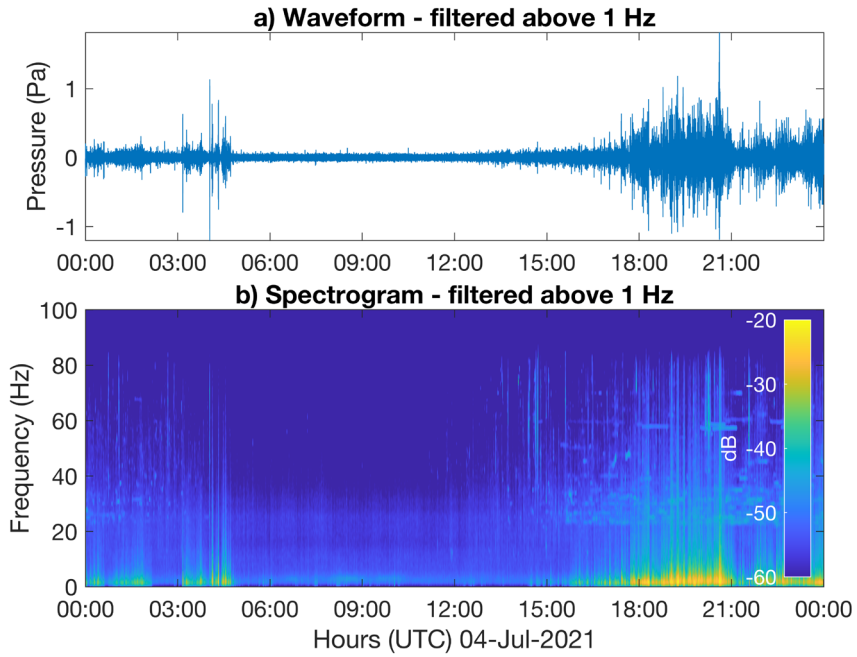
a) Waveform - filtered above 1 Hz
Pressure (Pa)
1
0
-1
00:00
03:00
06:00
09:00
12:00
15:00
18:00
21:00
b) Spectrogram - filtered above 1 Hz
Frequency (Hz)
100
80
60
40
20
0
dB
-20
-30
-40
-50
-60
00:00
03:00
06:00
09:00
12:00
15:00
18:00
21:00
00:00
Hours (UTC) 04-Jul-2021

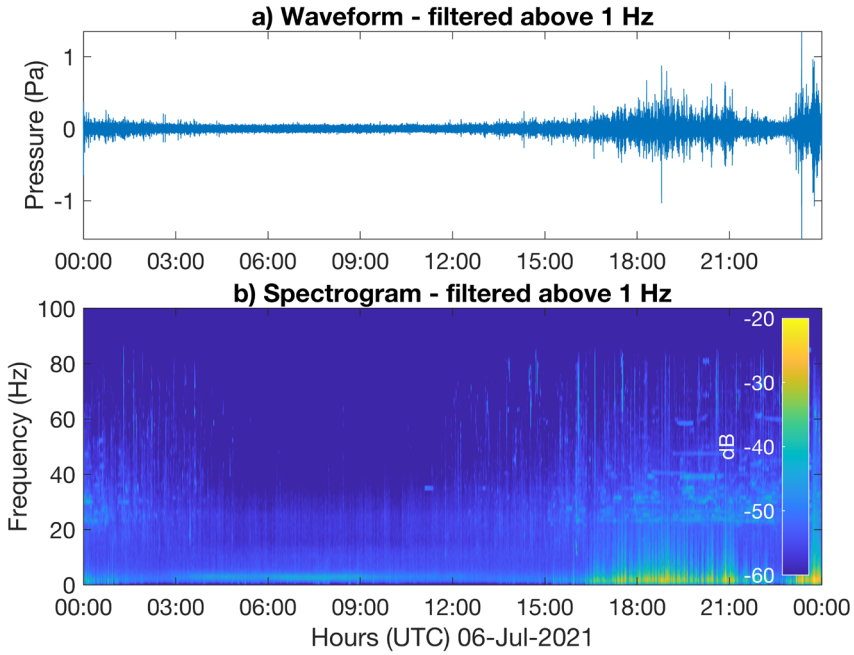
a) Waveform - filtered above 1 Hz
Pressure (Pa)
1
0
-1
00:00
03:00
06:00
09:00
12:00
15:00
18:00
21:00
b) Spectrogram - filtered above 1 Hz
Frequency (Hz)
100
80
60
40
20
0
dB
-20
-30
-40
-50
-60
00:00
03:00
06:00
09:00
12:00
15:00
18:00
21:00
00:00
Hours (UTC) 06-Jul-2021

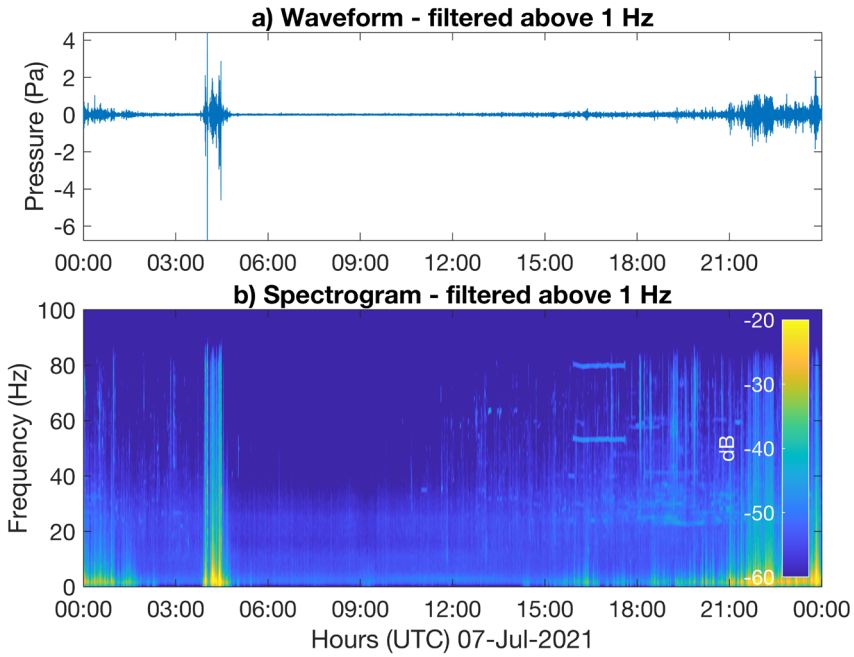
a) Waveform - filtered above 1 Hz
Pressure (Pa)
4
2
0
-2
-4
-6
00:00
03:00
06:00
09:00
12:00
15:00
18:00
21:00
b) Spectrogram - filtered above 1 Hz
Frequency (Hz)
100
80
60
40
20
0
dB
-20
-30
-40
-50
-60
00:00
03:00
06:00
09:00
12:00
15:00
18:00
21:00
00:00
Hours (UTC) 07-Jul-2021